Synthesis and fluid interaction of ultra long Carbon Nanotubes

by

Mario Hofmann

Submitted to the Department of Electrical Engineering and Computer Science

in Partial Fulfillment of the Requirements for the Degree of

Master of Science in Electrical Engineering and Computer Science

at the Massachusetts Institute of Technology

February 2009

Author_____
Department of Electrical Engineering and Computer Science
August, 2008

Certified

by_____
Jing Kong
Assistant Professor
Thesis Supervisor

Accepted

by_____
Terry P. Orlando
Professor of Electrical Engineering
Chairman, Department Committee on Graduate Theses

Synthesis and fluid interaction of ultra long Carbon Nanotubes

by

Mario Hofmann

Submitted to the
Department of Electrical Engineering and Computer Science

August 29, 2008

In Partial Fulfillment of the Requirements for the Degree of
Master of Science in Electrical Engineering and Computer Science

ABSTRACT

The successful integration for carbon nanotubes in future electronic applications relies on advances in their synthesis. In this work optimization of growth parameters was conducted to obtain ultra long carbon nanotubes. Their morphology was analyzed by means of different techniques and evidence of the occurrence of nanotube bundles was found. The effect of varying several parameters on the morphology of the obtained nanotubes was investigated and successful growth of ultra long nanotubes was achieved. The settling process, i.e. the sinking of the nanotubes to the substrate, of those nanotubes was investigated by a newly developed *in-situ* rotation tool and statistical data for their behavior during growth was obtained.

Thesis Supervisor: Jing Kong
Title: Assistant Professor, MIT Electrical Engineering and Computer Science

1. Introduction to Nanotubes 4
2. Experimental: Synthesis of long carbon nanotubes 7
2.1. Catalyst 7
2.2. Preparation 9
2.3. Deposition 10
2.4. Growth 10
3. Analysis 11
3.1. Scanning electron microscopy (SEM) 11
3.2. In-situ sample rotation 12
3.3. Atomic force microscopy (AFM) 13
3.3.1. AFM artifacts 15
Scan size 15
Applied force 16
3.4. Raman spectroscopy 17
3.5. Electrical measurements 20
3.6. AFM diameter distribution 22
3.6.1. Predictions for bundles (diameter, variance) 22
3.6.2. Application to experimental results 26
4. Optimization of carbon nanotube growth 28
4.1. Effect of the gasses 28
4.1.1. Pretreatment 28
4.1.2. Choice of gas 29
4.2. Conditioning of the reactor chamber 30
4.3. Optimization of Catalyst 32
4.3.1. Relation between catalyst size and nanotube size 32
4.3.2. Choice of catalyst 35
5. Fluid dynamics 37
5.1. Statistical analysis of aligned carbon nanotubes 37
5.2. Forces supporting a floating nanotube 40
5.3. Observations on individual nanotubes 43
6. Conclusions 48

1. Introduction to Nanotubes

Carbon nanotubes are a material of extreme contrasts. Even though they have been around for 10.000 years (ice core [1]) and are generated by natural gas flames [2] in every household they were first investigated in 1991 by Sumio Iijima [3].

The geometry presents another contrast inherent in carbon nanotubes: Typical single walled carbon nanotubes are cylindrical structures with a diameter of 1nm and can extend to lengths of up to 4cm [4]. This aspect ratio would correspond to a human hair (100um) being long enough to circle the MIT campus (Figure 1).

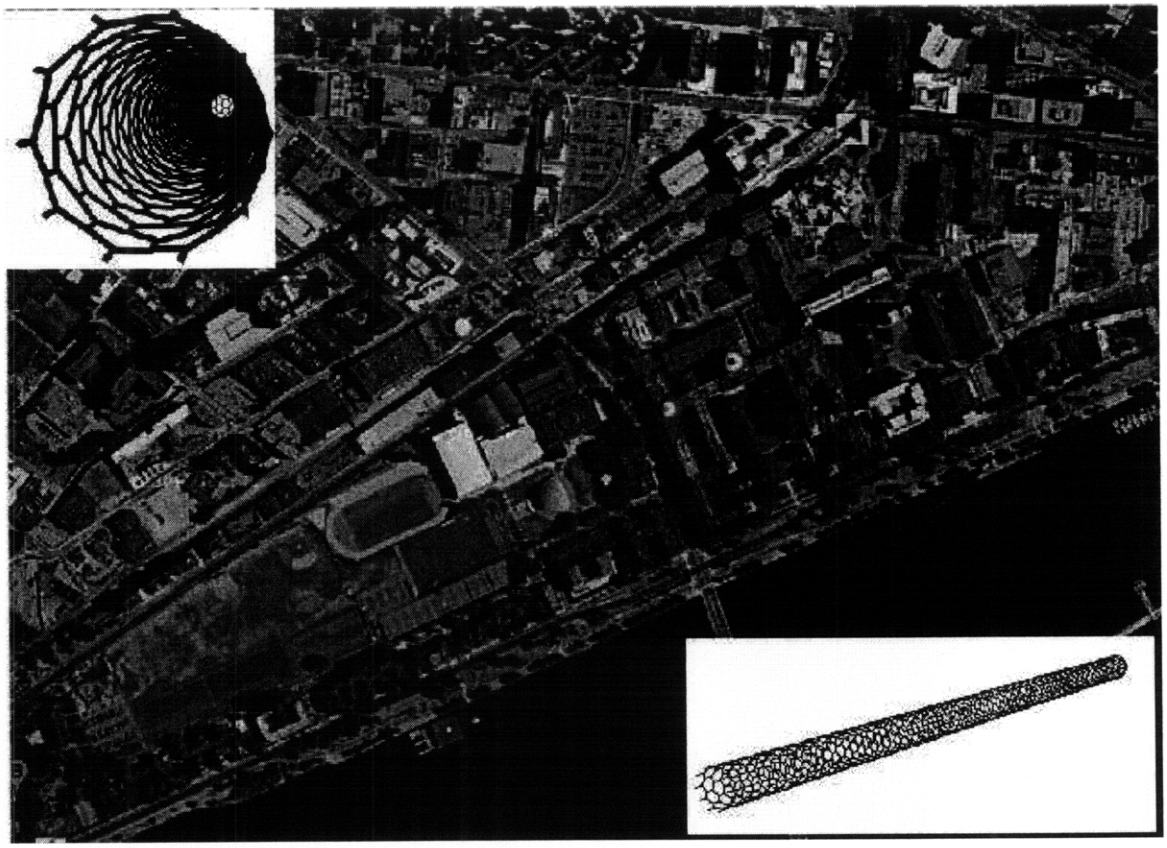

Figure 1 Image of MIT campus with circumference as described in text (insets) depiction of a singlewall carbon nanotube

The list of application of carbon nanotubes is extensive [5] and their unique properties can be explained by evaluating their structure:

To understand the structure of CNTs normally a thought experiment is employed and the reader is encouraged to imagine rolling up a sheet of sp^2-hybridized carbon, known as

graphene to form a cylinder. Since 2004 graphene can actually be generated and side-by-side comparison of the two structures is finally possible.

Both materials are remarkably resilient since the carbon-carbon-bonds they consist of, are known to be the strongest occurring bond. This gives them a mechanical strength that is unprecedented and opens possibilities as polymer reinforcements.

Carbon nanotubes, however, have an advantage that could make them superior in several respects – the absence of edges:

It was reported that graphene would preferentially exhibit armchair or zigzag edges [6] – conformations that are displayed in Figure 2 . Nanotubes however can be rolled up from graphene sheets with any intermediate chirality. Because of that there is a large variety of possible behavior in such fundamental respect as magnetism or spin transport.

Edges also provide a nucleation site for defects since atoms at these exposed areas are easier to remove. If the circumferential dimensions are starting to be significant –as expected for graphene nanoribbons- the chemical inertness as well as resistance to electromigration might become compromised by these defects.

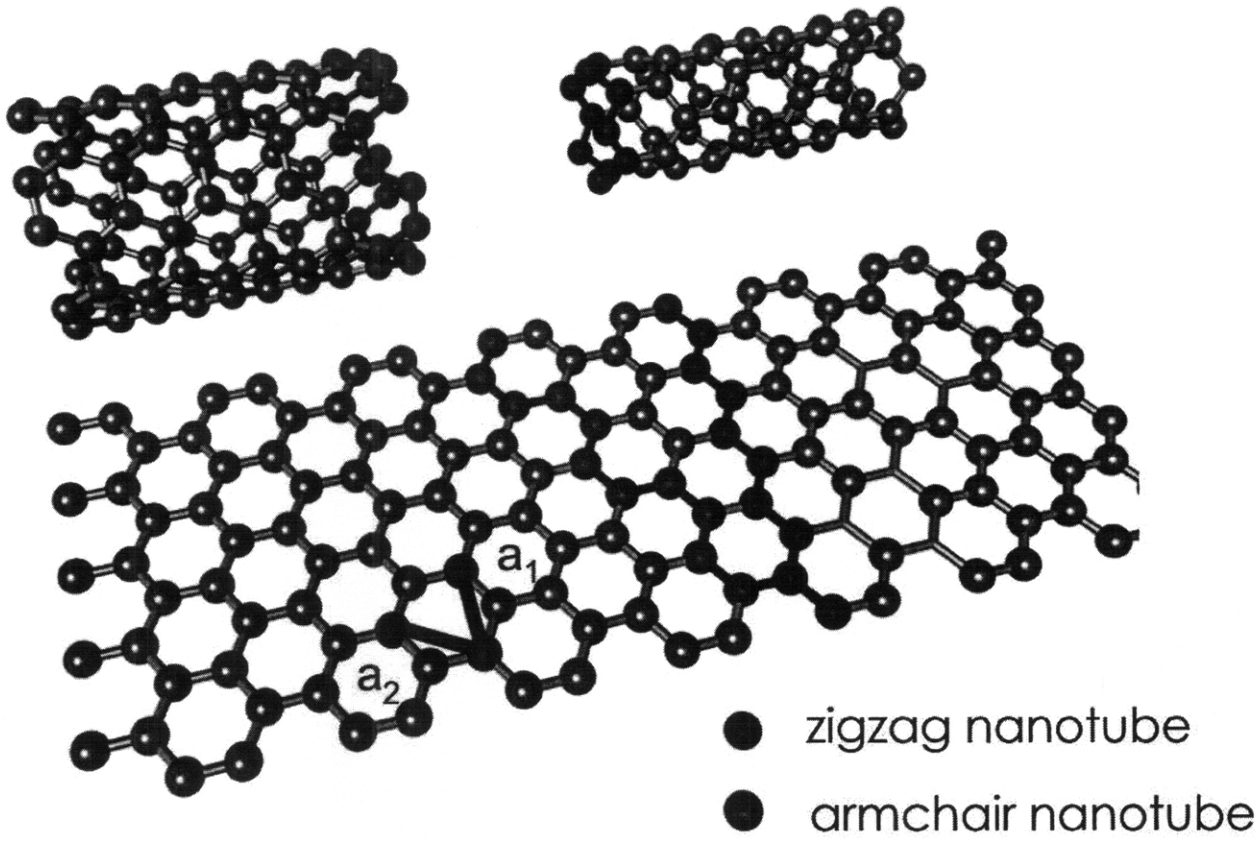

Figure 2 Graphene sheet and derrived carbon nanotubes

The electronic structure of both materials depends sensitively on their lateral dimensions: Since the wave function for nanotubes has to be continuous across the scroll seam only certain sets of states are allowed in circumferential direction. In Graphene nanoribbons the wave functions have to follow similar boundary conditions at the edges. Depending on the position of these allowed states to the K-point (the touching point of valence and conduction band) nanotubes can exhibit metallic or semiconducting behavior whereas nanoribbons are only semiconducting with a bandgap that depends on their width.

The choice whether to use nanotubes or graphene will eventually be affected not only by their intrinsic properties but also by the ease of use.

Graphene nanoribbons could rely on conventional synthesis infrastructures, since they provide a top down approach to controlling the electronic structure of a carbon based device. Carbon nanotube synthesis on the other hand relies on complex self-organization processes which can only be insufficiently controlled even after almost two decades.

We will attempt to provide more insight into the control of these processes in this thesis.

2. Experimental: Synthesis of long carbon nanotubes

A large variety of synthesis methods (laser ablation, arc discharge) has been reported over time but in the last years research has been focusing on chemical vapor deposition (CVD) as indicated in Figure 3. The ease of use might be a reason for this development. Furthermore the implementation of wet chemically derived catalyst or thin films is more suitable with this process than in other available synthesis methods. In this chapter the processing steps to generate carbon nanotubes are described.

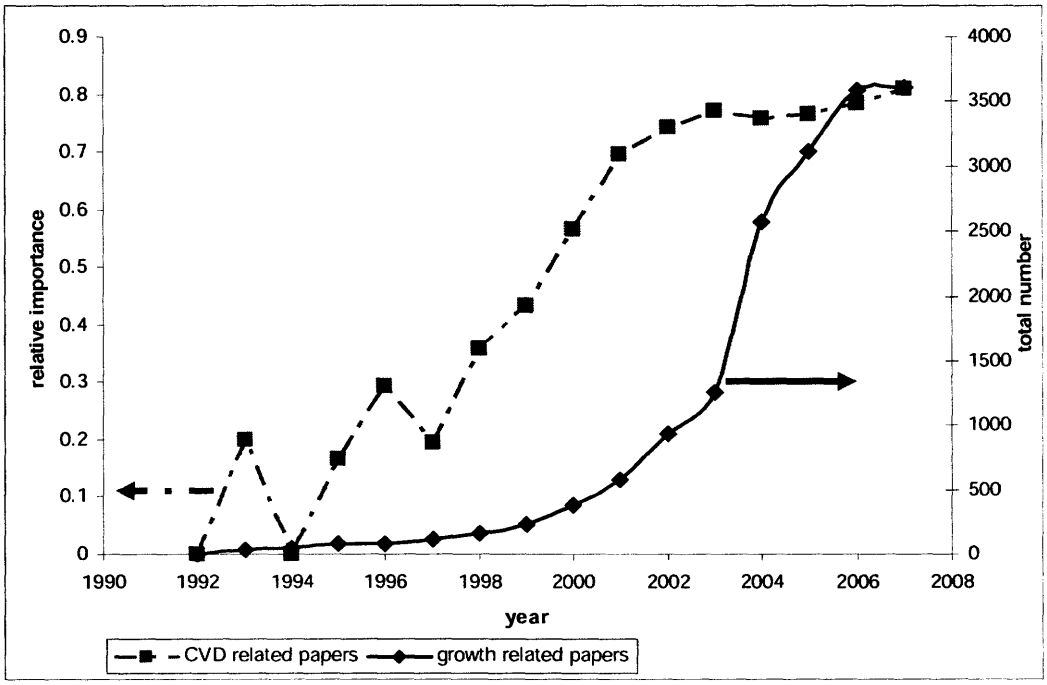

Figure 3 Relative significance of chemical vapor deposition (over arc discharge and laser ablation) and total number of publications concerning nanotube synthesis over time

It is also interesting to note that the amount of publications devoted to the synthesis of carbon nanotubes reached saturation 2 years ago, which might be related to the persistent problems of chirality controlled growth.

2.1. Catalyst

The catalytic material plays, arguably, the most crucial role in the CVD process. In thermal CVD it has a two fold function – it provides a low energy route to dissociating the carbonous precursor as well as incorporating these dissociated carbon products into the extruding carbon nanotube.

A compromise between the two tasks has to be found and the tailoring of catalytic material is an active research field.

The synthesis of ultra long carbon nanotubes has a further requirement as pointed out by us earlier: In order to sustain long time growth –the prerequisite for ultra long carbon nanotubes- catalyst deactivation has to be avoided. It was reported that this catalyst deactivation proceeds in a two step process: Upon uptake of carbon a liquidification of the catalyst particle occurs. If the carbon concentration becomes too larger the particle solidifies again and the efficient incorporation of carbon atoms into the nanotube cannot proceed anymore. Instead the particle is overcoated by amorphous carbon and the particle is deactivated.[7] There is discussion if liquidification occurs in large catalyst particles (>3nm) or if surface diffusion on a pure metallic cluster is the main growth route. However, irrespective of the details a solution to the issue of catalyst deactivation seems to be large catalyst particles.

It seems that fluctuations in the carbon concentration within the particle could be a reason for catalyst deactivation, since an "overdose" of carbon would irreversibly solidify the catalyst particle. In this case a large volume could average the effect of fluctuations and provide a more continuous carbon supply to the growing nanotube.

The overcoating of the catalyst surface by an excess of reaction products could also be remedied by a larger particle since the surface area would scale accordingly.

This approach has not been widely attempted because a correlation between catalyst particle size and nanotube diameter was expected: Several groups [8] [9] reported that large particles would only grow big diameter nanotubes which are not very desirable in the field of electronics.

However high resolution TEM investigation [10, 11] and subsequent theoretical analysis showed that the extrusion of a nanotube from a portion of the catalyst cluster was possible [12].

It was argued that an inhomogeneous carbon concentration could lead to reduced melting

temperature and higher mobility in a part of the catalyst particle. As saturation within this area increases the surface becomes unstable and perturbations on the surface can occur. The increase in curvature would result in an increased solubility of carbon in this area and if the radius of the perturbation exceeded a critical value the surface tension would be overcome and an irreversible extrusion of a bump on the catalyst would occur.

This process is limited by a number of occurring mechanisms: Decrease in catalyst mobility as carbon concentration increases, precipitation of carbon at the bottom of the protrusion (where carbon solubility is lowest) or carbon depletion of adjacent catalyst regions.

These complex self-organizing phenomena might result in a self-limiting process and could cause a narrow size distribution of the generated protrusions and thus nanotubes.

2.2. Preparation

Large catalyst clusters were generated by utilizing a water-in-oil emulsion. The catalytically active iron, in the form of an iron(III)chloride salt, was dissolved in deionized water (3mg/ml) and then stabilized by a surfactant (Sodium dodecyl sulfate 30mg/ml). This polar solvent was added to nonpolar Hexanes and vigorously stirred until a suspension was achieved. This mixture tends to segregate after a couple of hours but stirring the solution with a magnetic stir bar can stabilize it again.

Figure 4 Photograph of vials with different catalyst solutions (from left to right) $FeCl_3$ solution, Hexanes/$FeCl_3$ solution before stirring, segregated mixture, stable mixture

2.3. *Deposition*

After experimenting with different deposition methods (spraying, dip-coating, stamping) we use a dip-pen technique to put a strip of catalyst on a Si/SiO_2 sample. The ease of use, sufficient spatial resolution and flexibility in patterning make it a good choice for our application. In addition the hexanes is not compatible with most photoresists and thus doesn't allow lithographical patterning of catalyst islands on the substrate.

To generate higher density films of carbon nanotubes for efficient investigation by AFM more catalyst strips had to be deposited. This was achieved by dipping a brush in the solution and after pre-drying it, depositing it on the substrate perpendicular to the gas flow direction.

2.4. *Growth*

A typical CVD process can be grouped into several phases (see Figure 6): First the air within the quartz reactor is displaced by purging with Argon. During pretreatment the chamber is heated to the growth temperature while the catalyst is subjected to a reactive atmosphere that is intended to destroy the surfactant coating of the catalyst particles and change the catalyst morphology and chemical state. (Figure 5)

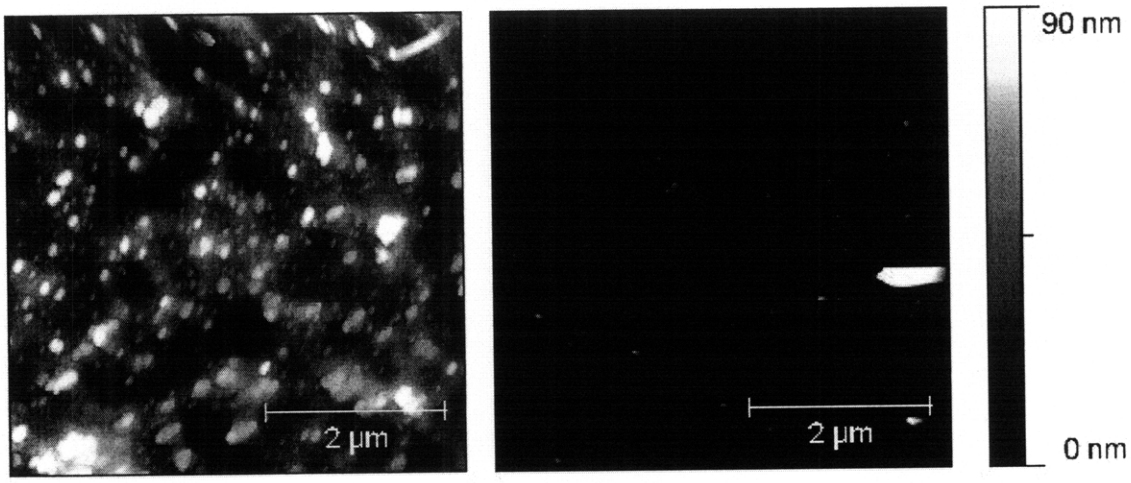

Figure 5 AFM images of catalyst before annealing (a) and after CVD (b) –observe same height scale

After pretreatment the carbonous precursor gas is injected into the reaction zone and the

growth initiates. The growth time can be varied according to the intended yield and normally ranges between 20 minutes to 1 hour.

During the cooling phase the reaction chamber is purged with Argon until the temperature is low enough to prevent oxidation of the grown nanotubes.

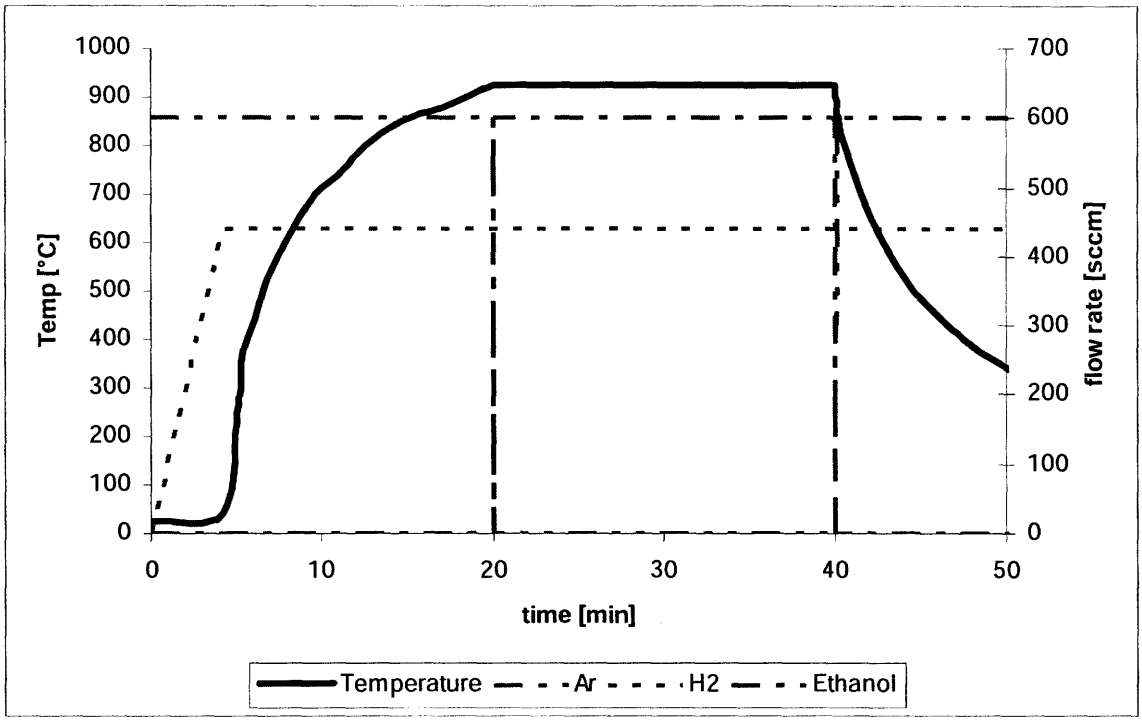

Figure 6 Measured Temperature and gas flow rates during CVD experiment

3. Analysis

The evaluation of a successful growth cannot be achieved by a single technique until now. Since a variety of properties is of interest for different applications we have to rely on a set of complementary analysis techniques that will be introduced briefly in the following chapter.

3.1. Scanning electron microscopy (SEM)

For the analysis of ultralong carbon nanotubes on insulating substrates Scanning electron microscopy (SEM) has been used as the primary tool. Even on large scale images carbon nanotubes can be identified as bright streaks on the SiO_2 substrate. This situation was explained by an electron transfer between the insulating SiO_2 and the CNT: The

secondary electron yield of the SiO_2 is decreased if the insulator is depleted by the electron beam induced current. The CNTs can supply this depeleted area by providing a conductive pathway to other regions. The secondary electron yield of a small area in contact with the CNTs can thus be recovered and CNTs are highlighted by a bright area around them.

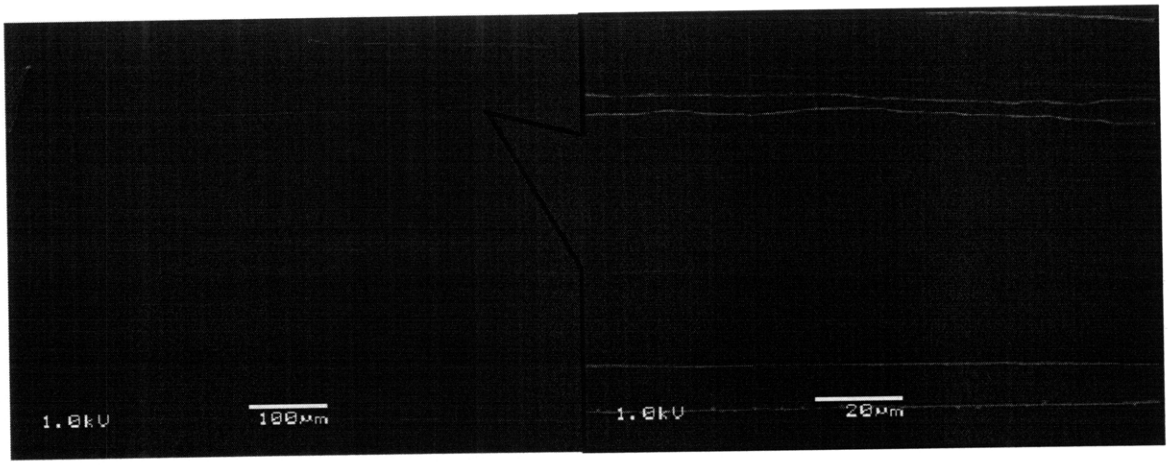

Figure 7 SEM image of ultralong flow aligned CNTs (a) low magnification (b) higher magnification (courtesy of Ying Feng)

3.2. In-situ sample rotation

Since ultralong nanotubes are represented as lines in the SEM pictures it is simple to extract their alignment angle. This inspired us to devise a setup that could infer on nanotube behavior from their alignment angle.

We use *in-situ* sample rotation as a tool to statistically investigate the behavior of about 10,000 long aligned nanotubes in a time resolved manner. Once a floating nanotube settles, it experiences a strong enough van der Waals interaction with the substrate so that it will not be affected by the gas flow anymore[13]. By changing the angle between the sample (to which the settled nanotubes are attached) and the gas stream direction that aligns the floating nanotubes, it is possible to distinguish between nanotubes settled before and after the sample rotation.

Figure 8 is a schematic diagram of the sequence of steps in our experiment and the resulting orientation of the nanotubes above or on the surface of the substrate. A complete experiment consists of 3 phases: (1) Carbon nanotube synthesis, after which the carbon feed stock is turned off; (2) an intermediate step in which all the nanotubes have

terminated their growth, while various perturbations to the settling process (such as cooling of the chamber or varying of the gas flow) are investigated; and (3) cooling to room temperature under Ar flow.

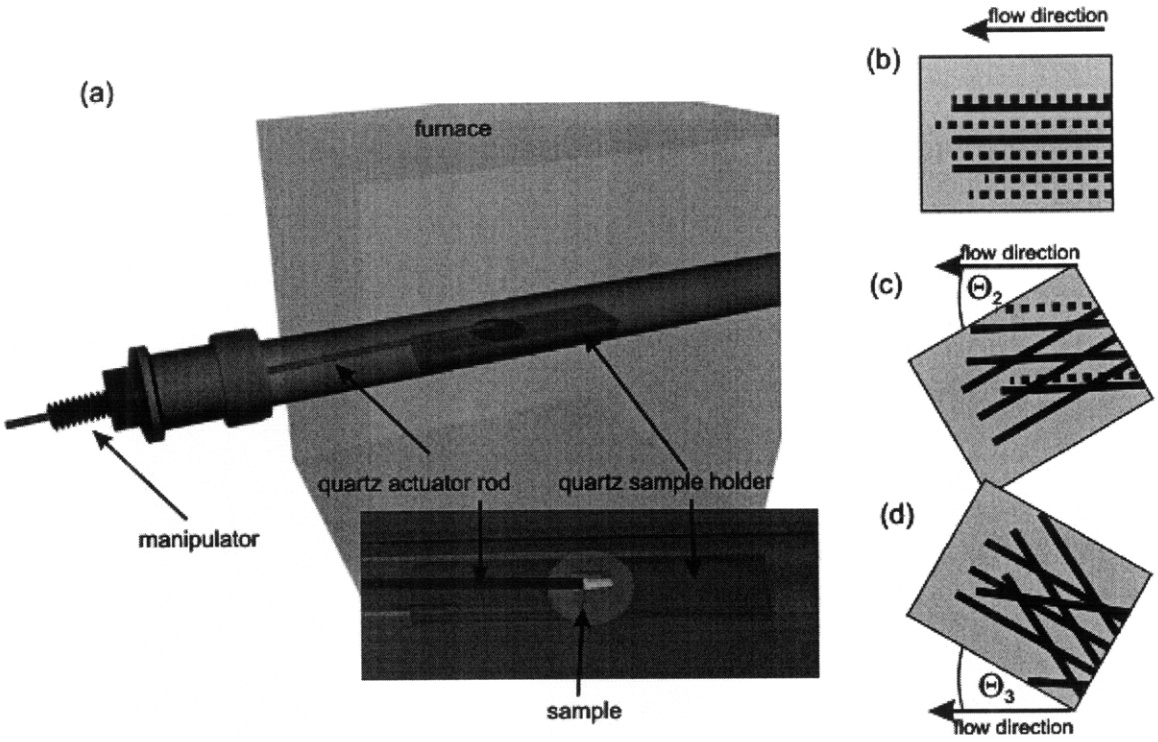

Figure 8 (a) Sketch of the experimental setup and (inset) photograph of the sample holder; (b-d) sample position and projection of settled nanotubes (solid lines) and floating nanotubes (dashed lines) on the substrate during experimental phases: (b) during growth, (c) during intermediate phase, (d) during settling phase

The gas flow direction relative to the substrate orientation in the growth phase is referred to as 0°. At the beginning of the intermediate phase (Figure 8c), the substrate is rotated to $\theta_2 = \sim 30°$ and all the floating nanotubes become aligned to this direction, and a number of them settle in this new direction. The third direction $\theta_3 = \sim -30°$ contains the rest of the floating nanotubes which settle during the cooling phase (Figure 8d).

3.3. Atomic force microscopy (AFM)

The general design of an atomic force microscope (AFM), developed by Binnig, Quate and Gerber in 1986, resembles a record player: A sharp tip attached to a cantilever is moved across the sample which interacts with the surface. Its vertical deflection is

amplified by a laser beam that is reflected from a mirror mounted on the tip. These deflections can be used to generate a 3D image of the topography.

Since nanotubes are only loosely attached to the substrate they can be moved on the substrate or even damaged if the AFM cantilever is exerting too much force on the sample. Tapping mode is one advance to resolve this issue: The cantilever is oscillated at a high frequency close to its resonance frequency by a piezoelectric actuator in the cantilever holder. The tip is then moved toward the surface until a vertical deflection of the cantilever occurs. A feedback loop is maintaining the same oscillation amplitude: When the cantilever encounters a bump the cantilever has less room to oscillate and the amplitude decreases. This is counteracted by the main piezoelectric actuator which will raise the cantilever holder until the amplitude is restored. The information of the piezo tube extension corresponds to the height image of the sample.

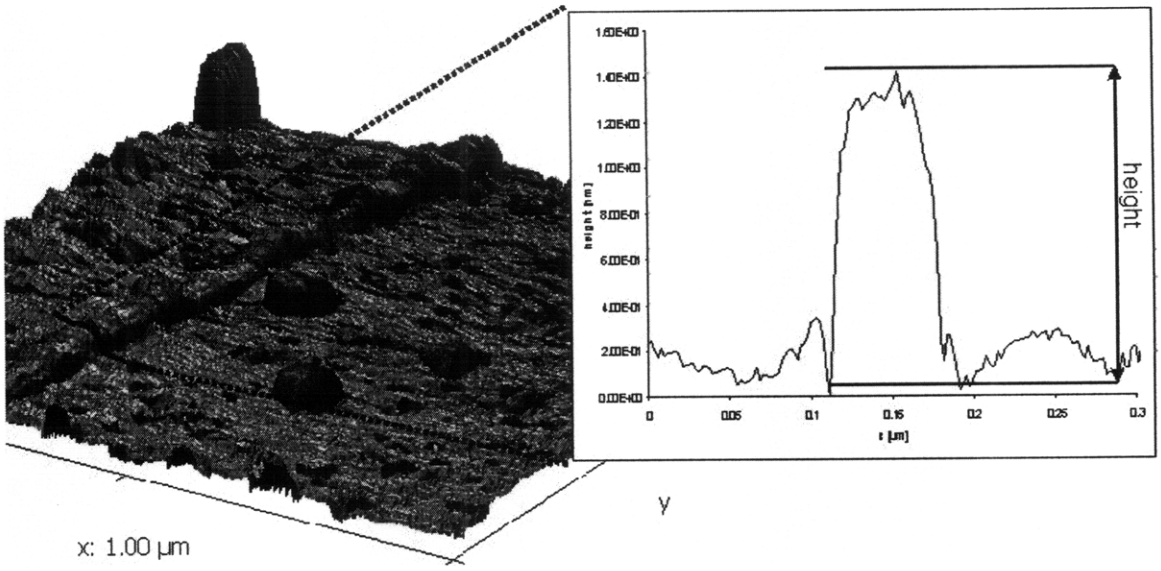

Figure 9 AFM 3D image of a nanotube and corresponding cross section

From this we extracted the height of a nanotube by subtracting the baseline from the highest point along the cross section.

At several instances split nanotubes like in Figure 10 were observed. The nanotube in this example was separated by scratching the sample after growth with a stainless steel needle. We can see that the original nanotube splits into two nanotubes which indicates that the nanotube originally consisted of more than one individual tube- a situation we call a nanotube bundle.

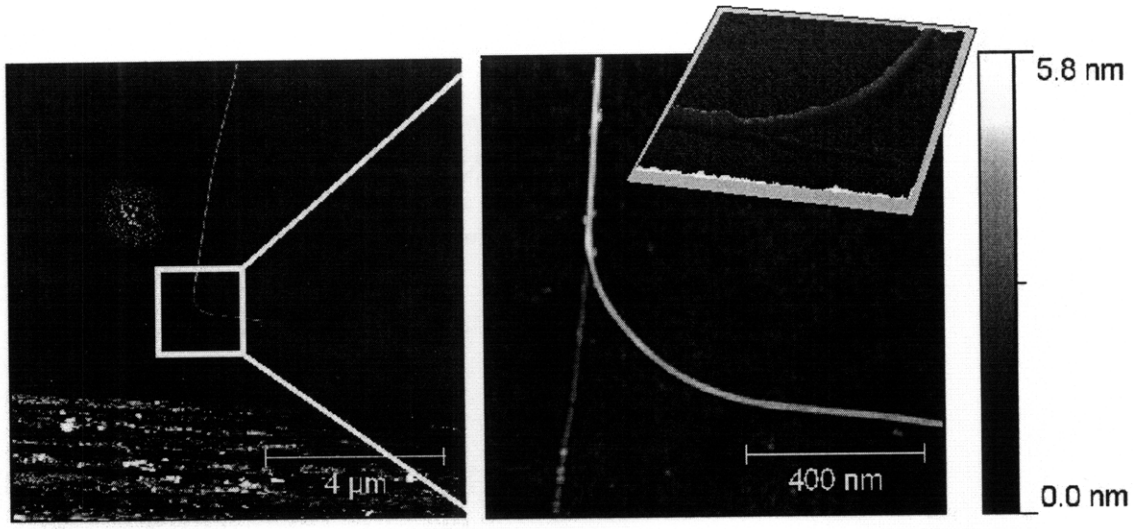

Figure 10 AFM image of a bundle that was split during mechanical agitation at different magnifications (inset) 3D representation

3.3.1. AFM artifacts

The obtained height image is affected by the choice of feedback loop and tapping force settings and their effect on nanotube images will be quickly reviewed.

Scan size

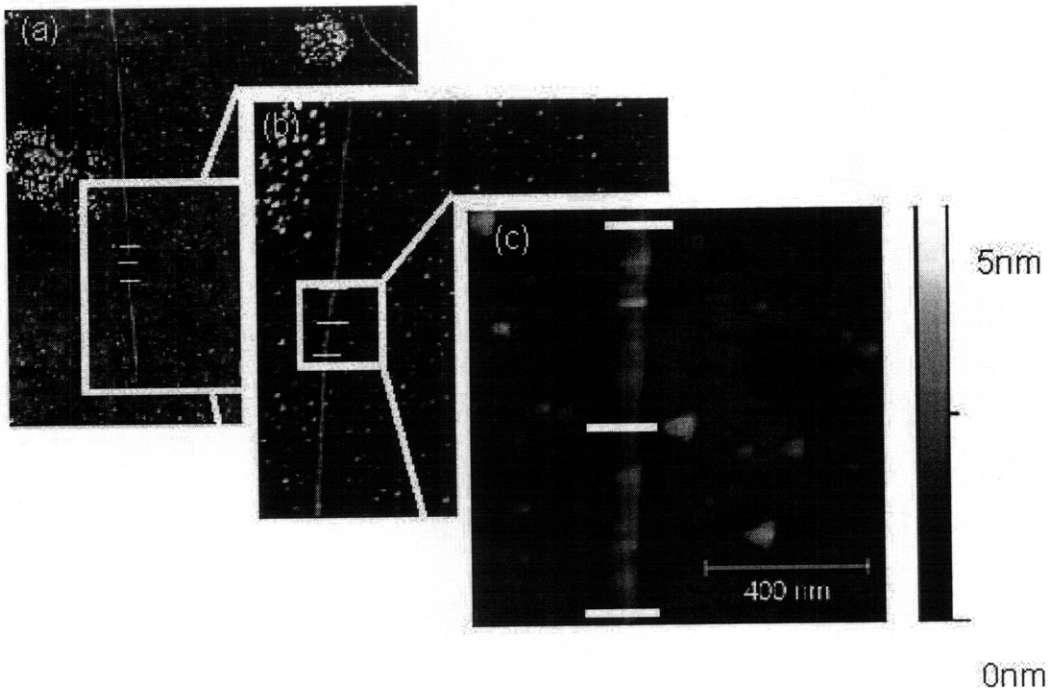

Figure 11 AFM height images of the same nanotube at different magnifications (a) 10um (b) 5um and (c) 1um size. The white lines correspond to positions where cross sections were taken.

The nanotube height is not very uniform as can be seen from the AFM images and so three points were identified at different length scales and the nanotube height was measured.

The average height was plotted versus the scan range size in Figure 12. The deviation between consecutive images is substantial but it can be seen that at larger scan sizes the nanotube height is overestimated. This can be attributed to limits of the feedback loop: At higher scan sizes the same feedback settings do not suffice to follow the contour of the nanotube as well. Instead the AFM tip lifts off of the sample as it encounters the nanotube and doesn't extend quickly enough to capture the actual height. Because of that a constant scan range should be chosen to be consistent.

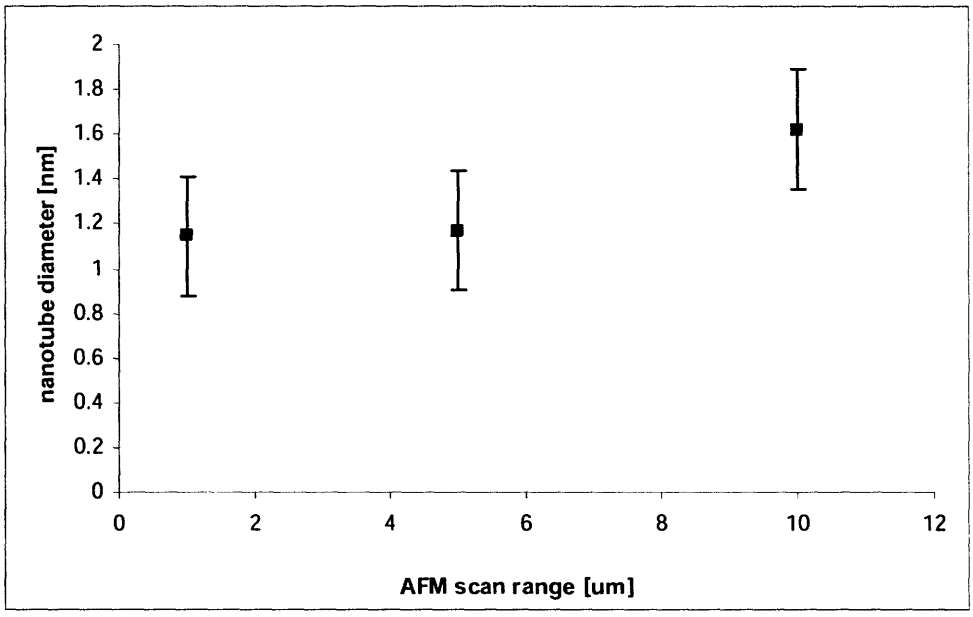

Figure 12 Nanotube height dependence on AFM scan size.

Applied force

Another artifact that influences the measured height of a nanotube is related to the exerted force: It was reported that the AFM tip can deform a nanotube by van-der-Waals interaction [14]. This behavior is captured in Figure 13: The amplitude setpoint (which

defines the vertical deflection signal of the photodiode and is thus inversely proportional to the force) is plotted against the average nanotube height (obtained at other positions than Figure 12).

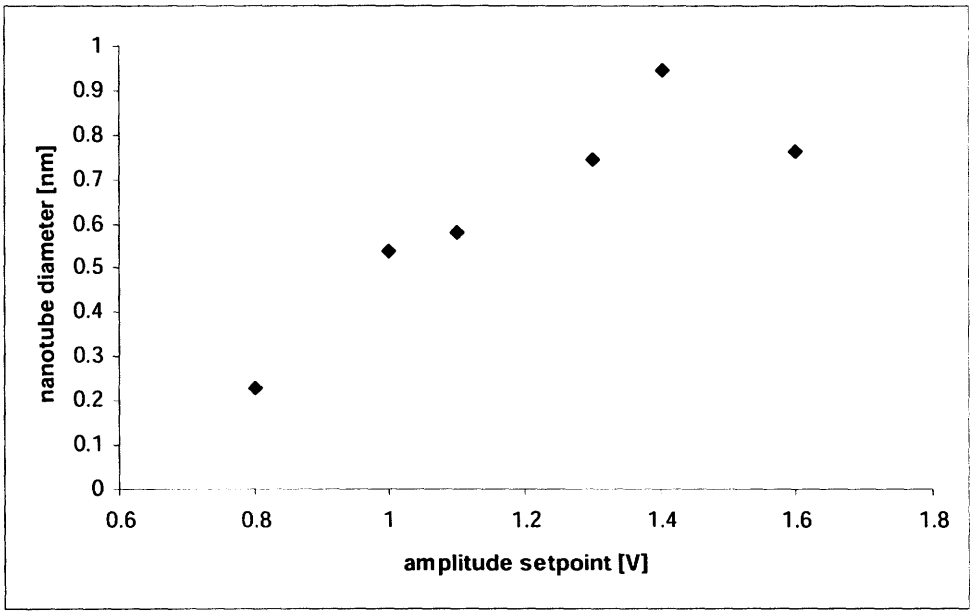

Figure 13 Nanotube height dependence on tapping force

It can be seen that a significant decrease in measured nanotube diameter occurs as the amplitude setpoint decreases below a threshold.

3.4. Raman spectroscopy

Raman spectroscopy has proven to be a quick and versatile method to identify morphology and character of a carbon nanotube. Figure 14 shows a matrix of Raman spectra taken in a scanning pattern. The color scale corresponds to the integrated intensity of the G-band. This feature is associated with carbonaceous material and the Raman map reflects the morphology of nanotubes.

From the same spectra the semiconducting or metallic behavior can be inferred and the RBM peak can be related to the diameter of a certain nanotube using the formula $\omega_{RBM} = \frac{217.8}{d} + 15.7$ [15].

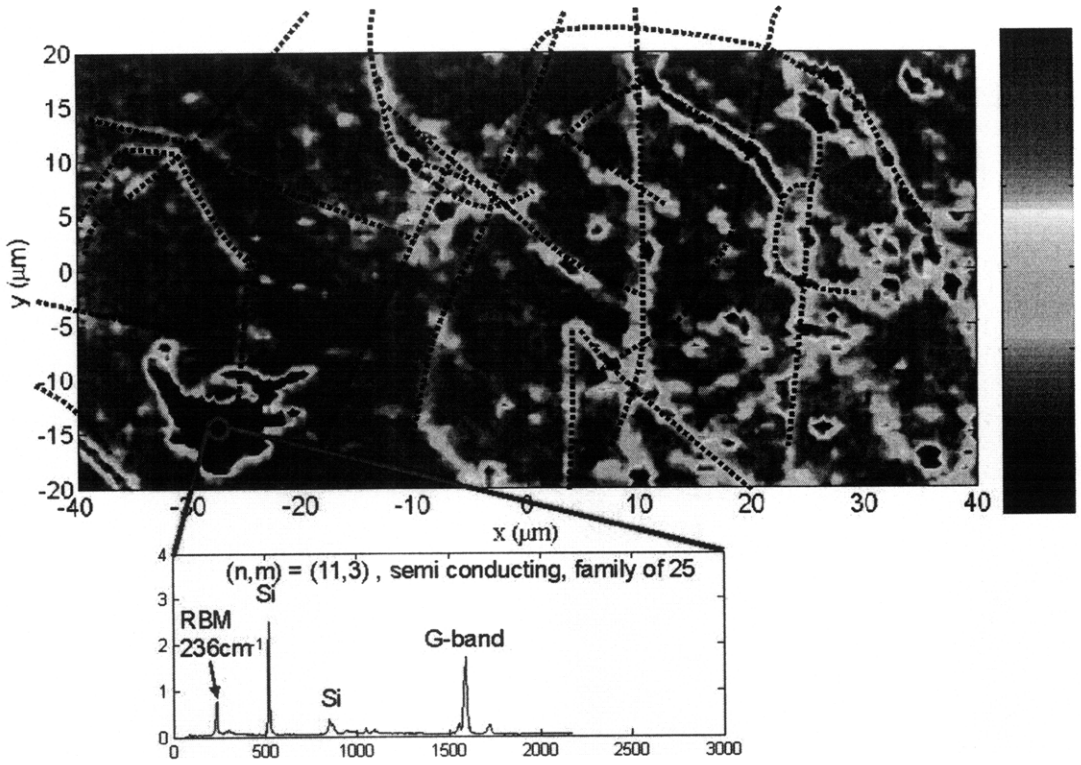

Figure 14 Raman map of integrated G-band intensity taken at laser energy 1.62eV and identification of a nanotube chirality (courtesy of Hyungbin Son (2007))

One drawback for spectroscopic analysis of nanotube ensembles, however, is the effect of resonance enhancement of individual nanotubes: The scattering cross section of nanotubes that have a transition energy in resonance with the excitation energy will be enhanced drastically whereas nanotubes far from resonance will not be detected.

To obtain a reliable diameter distribution a wide range of excitation energies has to be used and the same area has to be mapped for each laser line. This is a big task and cannot be done routinely to estimate the occurring diameters. However, it can be used to check the viability of using other techniques to obtain correct diameter distributions. The Raman diameter distribution in Figure 15 was obtained by investigating the RBM features of 275 different nanotubes using 7 excitation energies.

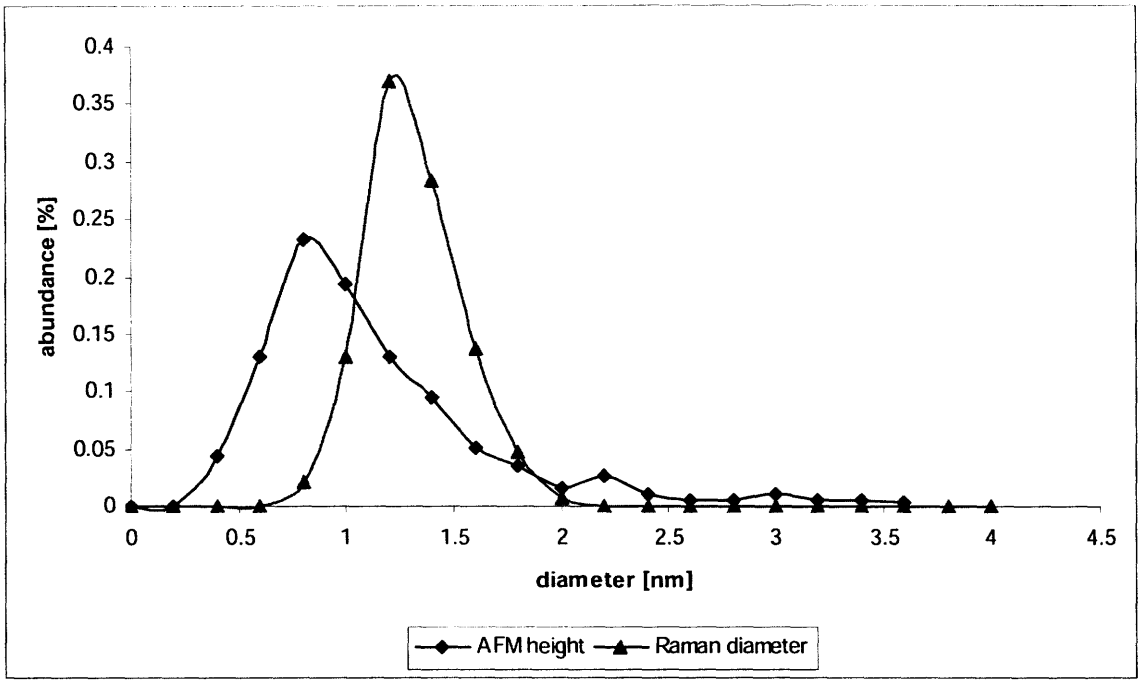

Figure 15 Comparison of diameter distributions obtained by AFM and Raman spectroscopy (courtesy of Ya-Ping Hsieh)

Figure 15 shows the diameter distribution of the same sample identified by Raman and AFM measurements. The diameter distribution obtained by Raman can be fitted to a Gaussian distribution with a goodness of r^2=98.3%).

The two techniques correlate remarkably well but some features require explanation:

It seems that the AFM distribution is shifted by 0.4nm with respect to the Raman distribution. A first hypothesis was that this could be due to the deformation of a nanotube on substrate by van-der-Waals interaction. However it was calculated that the radial compression would scale with diameter [14] and thus the difference at small diameters would be even more pronounced. It seems that this deviation could be related to the already explained imaging artifact induced by high tapping force.

Also the large diameter tail of the AFM distribution is not captured by the Raman distribution. This can be caused by two different scenarios: The RBM features for large diameter nanotubes cannot be resolved by the spectrograph since the Rayleigh scattered light interferes with the detection of the low energy Raman mode.

We however think that the absence of the larger nanotubes is caused by bundling: Raman spectroscopy probes nanotubes at an individual level and within a bundle only the

resonant nanotubes would contribute to the signal. AFM height distributions, on the other hand, will measure the size of the whole bundle.

We can see this behavior in Figure 16 where the Raman spectrum of the nanotubes within a single spot is shown. Two RBM peaks can be observed which indicates that two nanotubes are in resonance. These nanotubes cannot be distinguished by AFM and the diameters are not compatible with a double walled carbon nanotube and suggest a bundle.

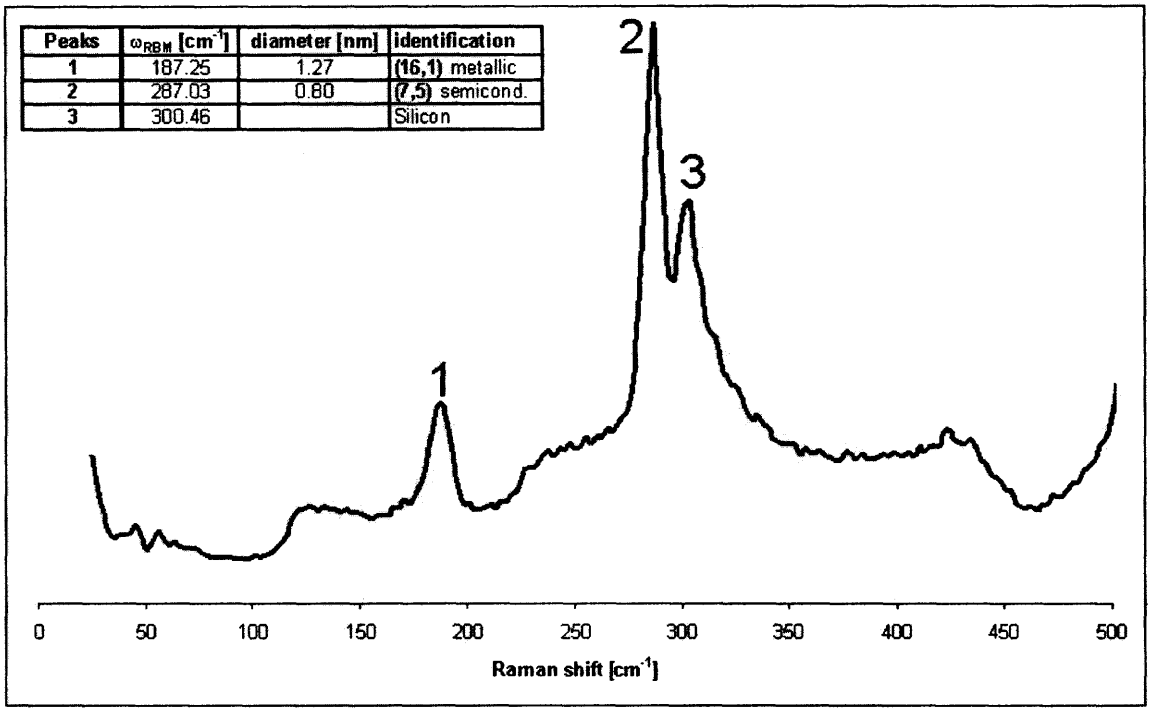

Figure 16 RBM region of a potential nanotube bundle (courtesy of Ya-Ping Hsieh)

3.5. Electrical measurements

Nanotubes synthesized with the described recipe were electrically contacted by depositing Au-electrodes on the grown nanotubes (as shown in Figure 17). After the lithography steps the morphology of nanotubes was investigated by SEM and single nanotubes were identified. Figure 18 shows the current-voltage-characteristic as recorded.

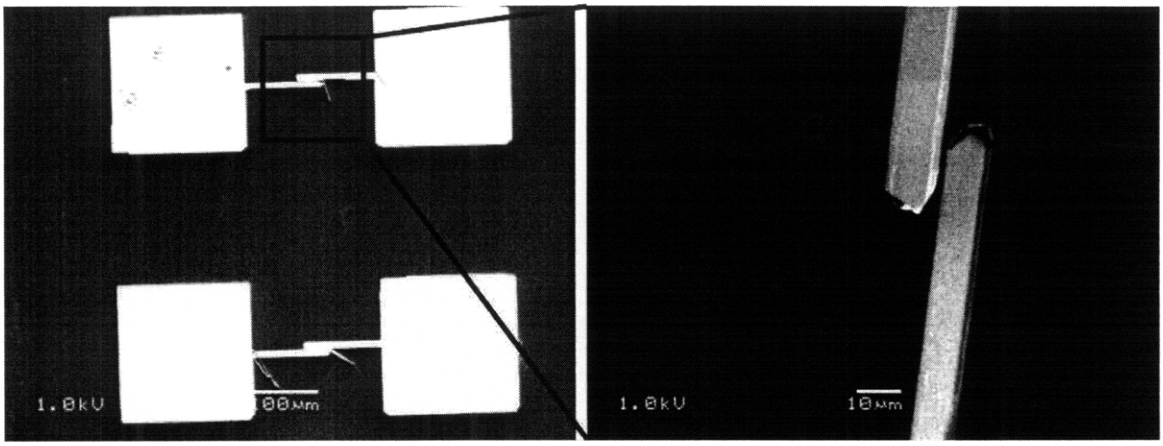

Figure 17 SEM picture of electrical devices of parallely aligned ultralong carbon nanotubes and closeup (courtesy of Hootan Farhat)

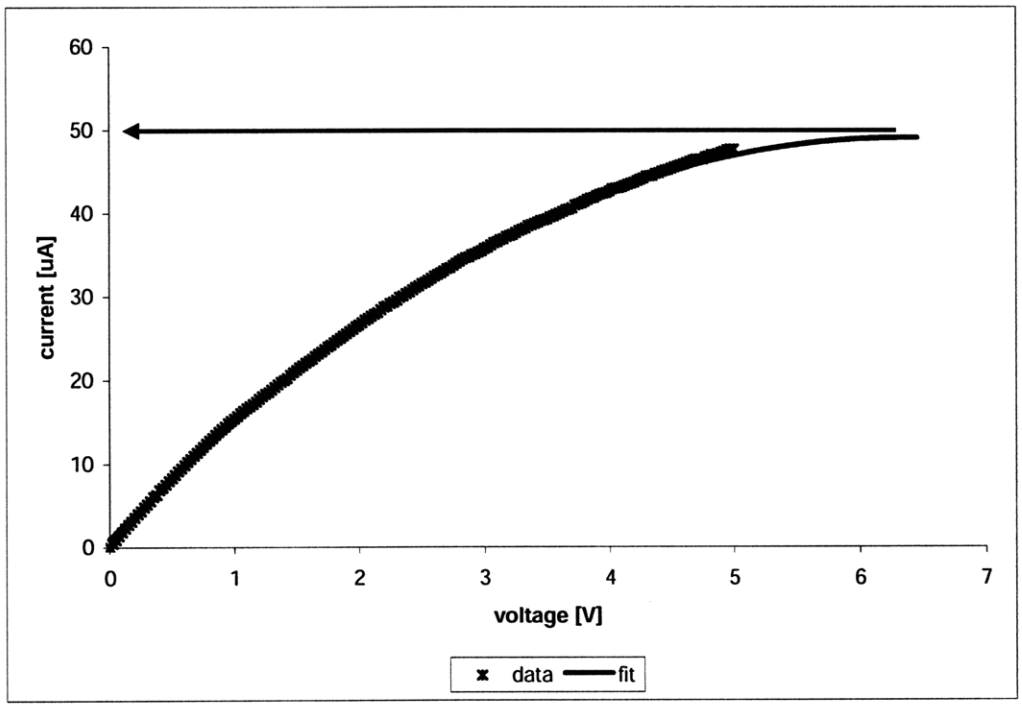

Figure 18 Current-Voltage characteristics of a nanotube device (courtesy of Hootan Farhat)

It can be seen that the current reaches saturation when a voltage larger than 5V is applied. This is attributed to the onset of efficient scattering due to the generation of optical phonons[16]. The saturation of an individual nanotube was found to be 25uA [17] but in our case the saturation current is about 50uA. This indicates that two carbon nanotubes are contributing to the conduction.

The dependence of the drain current on the gate voltage is shown in Figure 19 and the

observed device exhibits a large hysteretic behavior.

This difference between the forward and backward sweep was previously observed in both individual nanotubes and bundles and attributed to trapped charge states due to water or solvent residues.[18]

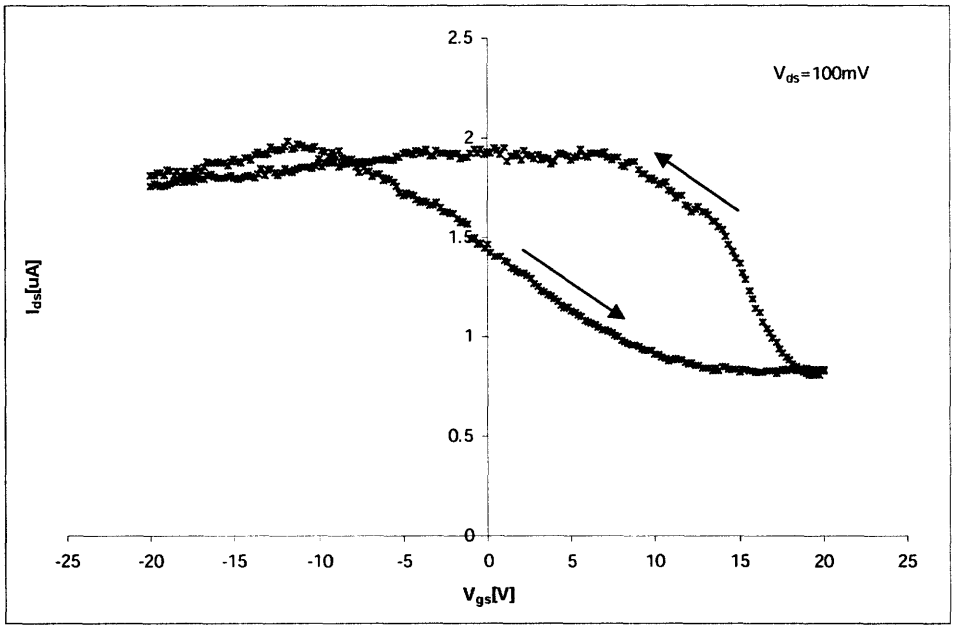

Figure 19 Gate sweep of a carbon nanotube bundle device

The hypothesis that a bundle is observed can be supported by the observation of a p-type behavior of the nanotube indicating a semiconducting nanotube and the low ratio of on- and off-current suggesting that a metallic nanotube is present.

This configuration raises the question how charging a metallic nanotube with a large number of available states is affecting the gate coupling of the semiconducting nanotube.

3.6. AFM diameter distribution

The hypothesis that our growth is yielding at least a portion of carbon nanotube bundles has been supported by a number of different observations and we will now investigate how bundles could be identified in AFM diameter distributions.

3.6.1. Predictions for bundles (diameter, variance)

Carbon nanotubes within a bundle are expected to adhere to one another by quite substantial van-der-Waals forces[19]. To maximize the contact area the resulting arrangement will resemble a hexagonally close packed (hcp) structure[20].

Thus the height of a nanotube bundle will be determined both by the diameter of the constituents as well as the number of layers involved.

The calculation for the dependence of bundle height on the number of layers for equal diameter constituents is straight forward and the result is plotted in Figure 20. In the same diagram the result of a numerical simulation is shown. This simulation captures the more realistic scenario that the nanotube diameters are varying within the bundle. The geometry is more involved (as can be seen in Figure 21 b) and a numerical solution is preferable. For this calculation n layers of nanotubes were consecutively stacked on top of each other and the resulting average height as a function of layer number was calculated for an ensemble of 10^6 nanotubes per layer.

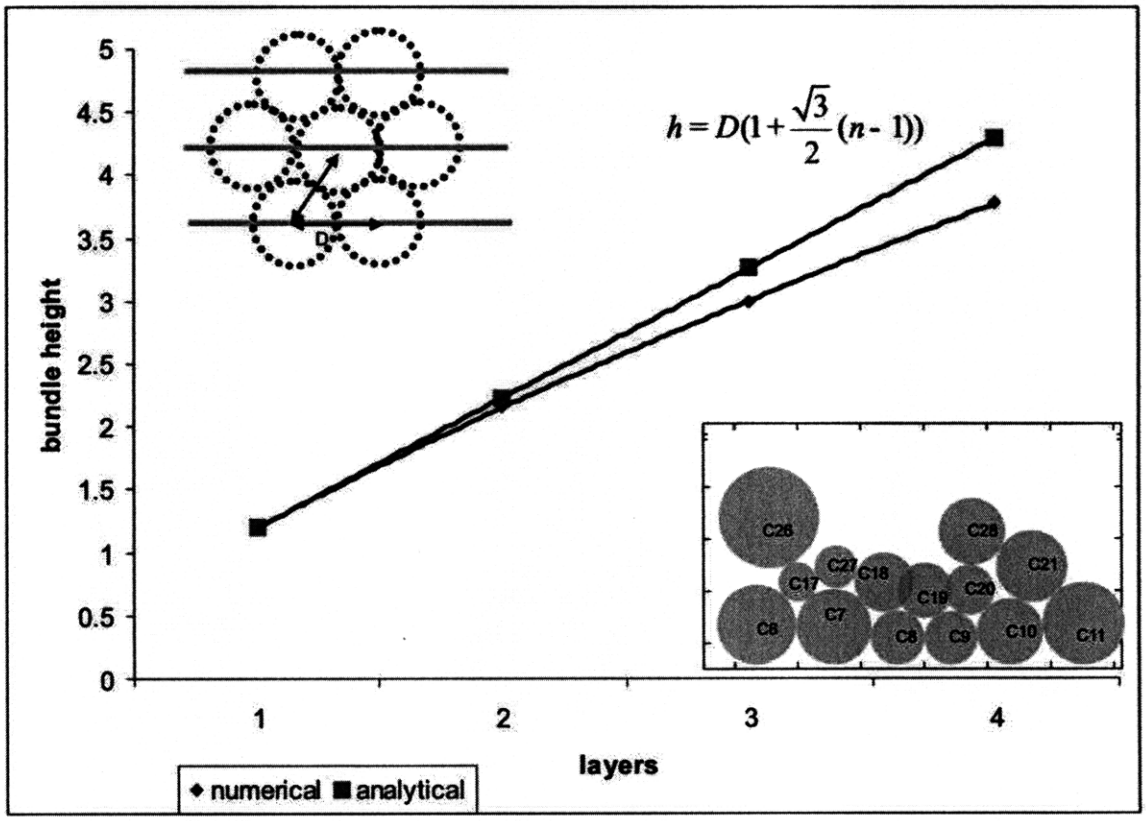

Figure 20 Diameter of bundles with different number of layers

These results of the analytical model agree remarkably well with the numerical and will

be used subsequently.

The variation of bundle height due to variation in nanotube diameters becomes larger as more layers of nanotubes are involved:
Looking at the diameter distribution obtained by Raman spectroscopy we can assume that the diameter of an individual nanotube follows a Gaussian distribution f .

$$f = \frac{1}{\sigma_1\sqrt{2\pi}} e^{\frac{(t-\mu_1)^2}{2\sigma_1^2}}$$

A second layer of nanotubes would increase the height variance more significantly than the first layer. That is because both their position and diameter would be uncertain: The nanotubes of the second layer would be supported by the first layer –giving them a distribution of center positions f- and their diameter would follow a second Gaussian distribution g (see Figure 21 a).

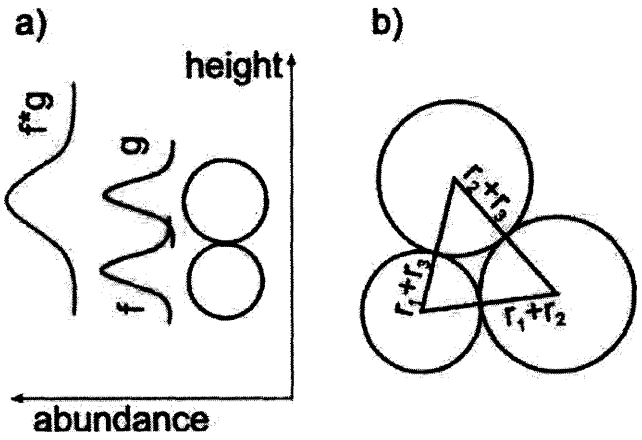

Figure 21 (a) Contribution of two carbon nanotubes to height variance in top stacked bundle (b) geometry for close packed bundle

This situation can be mathematically described by a convolution of the two distributions.

$$f * g = \frac{1}{\sqrt{2\pi(\sigma_1^2 + \sigma_2^2)}} e^{\frac{[t-(\mu_1+\mu_2)]^2}{2(\sigma_1^2+\sigma_2^2)}}$$

The resulting variance would be related to the diameter variance by

$$\sigma = \sqrt{\sigma_1^2 + \sigma_2^2}$$

However this result is only valid for the special case that two nanotubes are stacked exactly on top of each other. It is more likely that a closed packed structure between consecutive layers occurs.

In this case we have to rely again on numerical simulations and the average height for the described stacking procedure is shown in Figure 22.

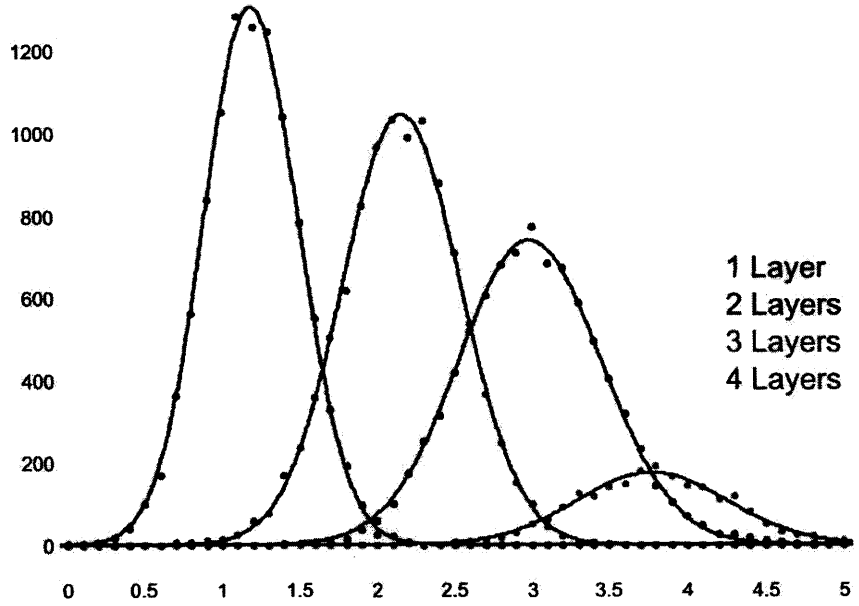

Figure 22 Height histogram for different numbers of layers and fit to Gaussian distributions

The height histogram in can be fitted with Gaussian distributions for different number of layers and the variance of this distribution was then related to the initial diameter distribution. The result is shown in Figure 23.

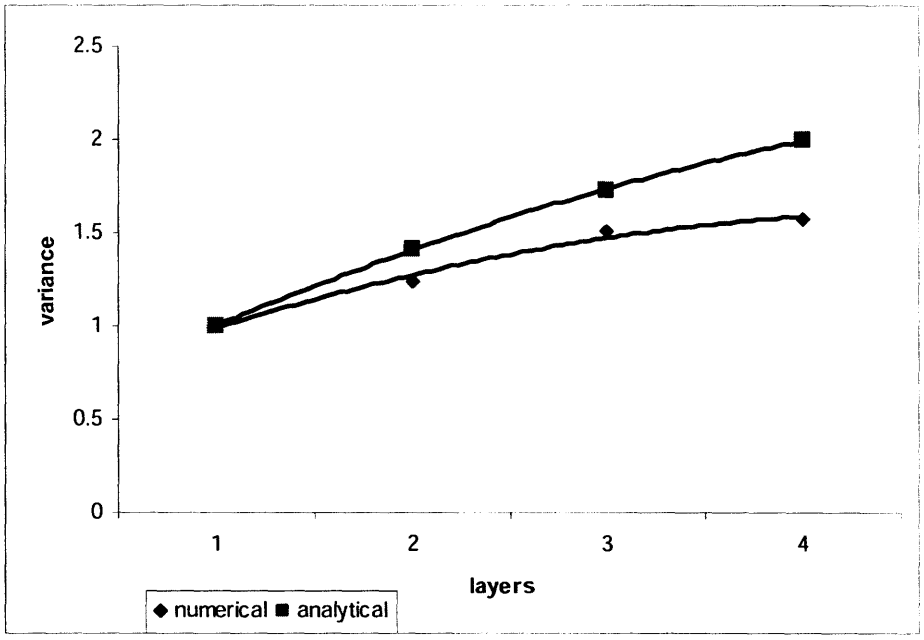

Figure 23 Variance of Gaussian distributions fit to bundle height for different number of layers

It can be seen that the analytical prediction overestimates the change in variance due to closed packing. The small changes in variance as the bundle gets larger can be explained by considering the bundle geometry: A nanotube can only be added to a new layer when the gap sizes of the underlying nanotubes are smaller than its size. Otherwise the nanotube will fill this gap and be integrated into the previous layer. Because of that the variance cannot exceed the nanotube diameter.

3.6.2. Application to experimental results

We expect the AFM height histogram of carbon nanotube bundles to consist of contributions from bundles with different thickness. As explained the difference in the number of layers as well as the diameter distribution of individual nanotubes is going to affect the resulting height distribution. Figure 24 shows the deconvolution of an AFM height distribution of 542 nanotubes into 6 peaks. The only restriction to the fitting procedure was the increase of variance for higher number of layers. The correlation between the first peak (indicating the contribution of individual nanotubes to the first layer height) and the previously described Raman size distribution is remarkable. This is very surprising since neither the position nor the width of the first peak was restricted but

only the overall goodness of fit to the experimental data was maximized. This supports our hypothesis that the observed nanotubes are grouped in bundles. Raman spectroscopy would probe the individual nanotubes which have a size of 1.34nm and a FWHM of 0.5nm

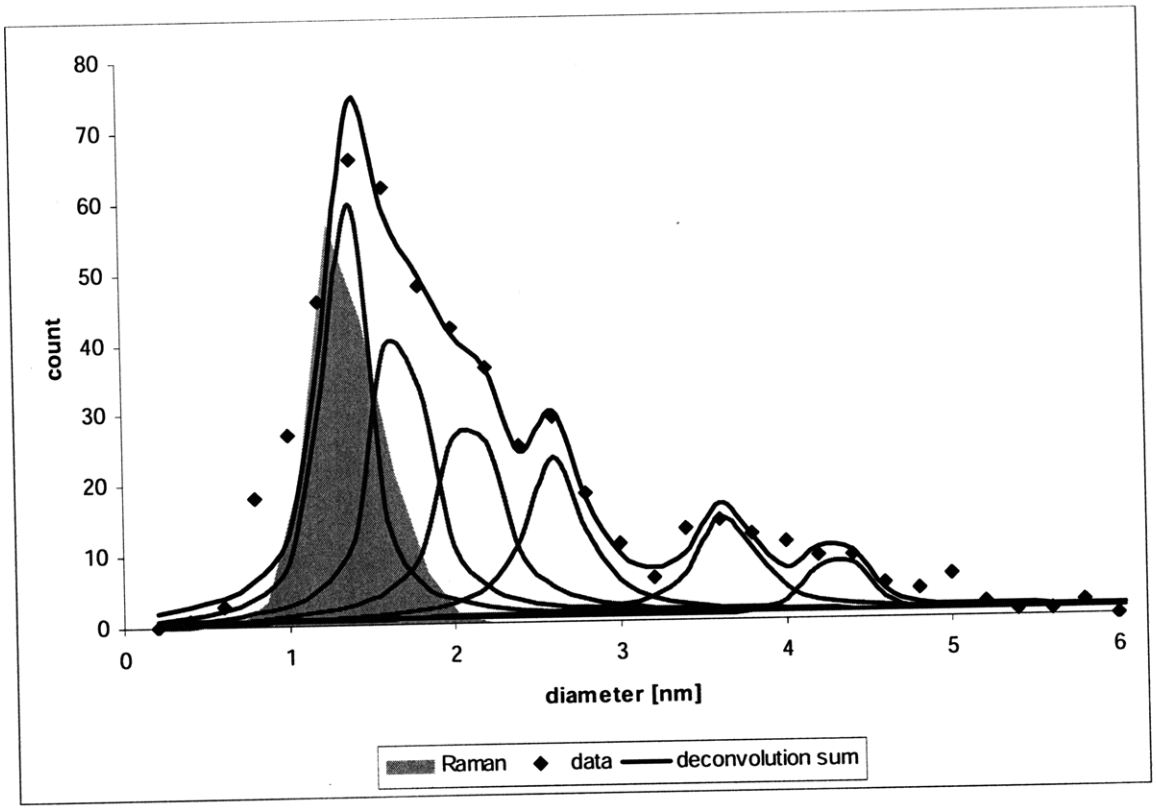

Figure 24 Example of AFM height histogram with deconvolution and previously described Raman diameter distribution

The following Table 1 shows how the different explained variances are affecting the quality of the fit: If the peak width is not changed between consecutive layers the resulting fit does not reflect the experimental data as well as for the cases of varying peak width.

The described analytical solution for the variance of bundles is very close to the results obtained by the numerical solution but the last fit is marginally better.

Table 1 Goodness of fit for different variances

		Peaks					
variance	**χ^2**	**1**	**2**	**3**	**4**	**5**	**6**
same gaussians	**0.9171**	1.34	1.67	2.1	2.62	3.66	4.32
analytical solution	**0.8853**	1.34	1.68	2.1	2.6	3.65	4.29
numerical solution	**0.8849**	1.34	1.68	2.1	2.61	3.65	4.31

One interesting observation is that the position of the deconvoluted peaks does not shift significantly for the different fitting strategies.

4. Optimization of carbon nanotube growth

Ultra long carbon nanotube growth is only achievable after optimizing a multitude of process variables. It was found that the main difference between short, randomly oriented nanotubes and long, aligned ones is the extension of catalyst lifetime. A careful balance of temperature, gas composition and catalyst chemistry has to be found to achieve this goal.

4.1. Effect of the gasses

The different gasses within the reaction zone have different functions: Argon as a noble gas does not take part in the chemical reactions but displaces oxygen and carries the carbonous feedstock. Hydrogen is used before growth to reduce the catalyst, which in ambient air occurs as oxides, and is also expected to influence the surface mobility of the catalyst clusters and affect their morphology.

The importance of the pretreatment has been shown by our group previously[21] but recently we investigated the possibility to synthesize carbon nanotubes from Copper and we will illustrate the effect of pretreatment in the next paragraph.

Hydrogen also acts as a reducing agent for amorphous carbon. This can prevent overcoating of the catalyst particles with dissociation products and keep the catalyst particle active for longer times[22].

4.1.1. Pretreatment

Only recently the successful growth of high yield carbon nanotubes using Copper

Chloride as a catalyst has been reported.

By screening a large parameter space we found that this synthesis is very sensitive to the pretreatment and choice of carbon precursor. The following table shows the results of different precursors and pretreatment steps.

		pretreatment		
		Ar	$Ar+H_2$	$Ar+H_2O$
growth	$Ar+H_2+Ethanol$	+	0	film
	CH_4	0	0	
	$Ch4+H_2$	++	+	

Table 2 Resulting growth using different pretreatment steps and growth methods (0-no nanotubes, + low yield, ++high yield)

One interesting result is the change in morphology upon addition of water in the pretreatment step: The carbon nanotubes seem to form a film throughout the sample (See Figure 25).

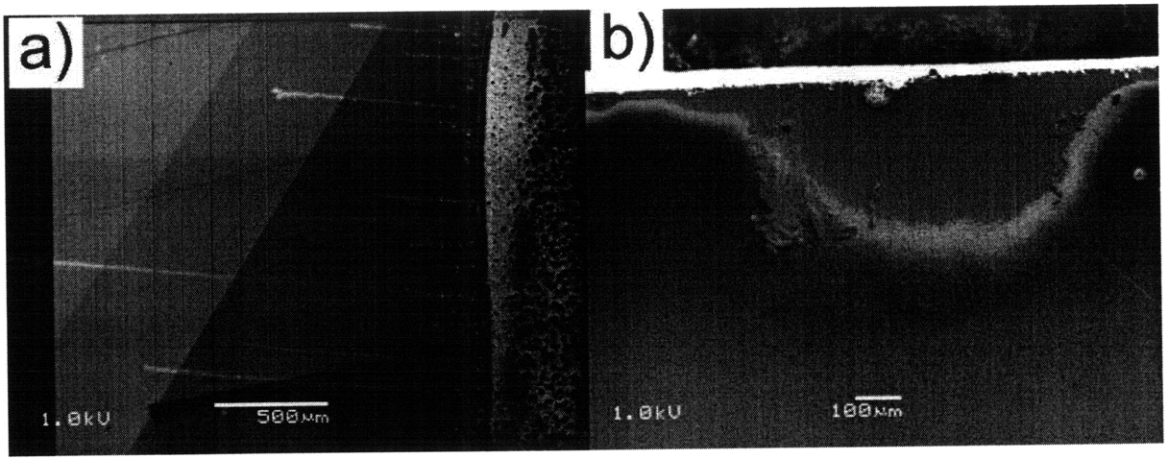

Figure 25 (a) SEM image of a high yield copper catalyzed growth, (b) filme of nanotubes generated by addition of water during pretreatment

4.1.2. Choice of gas

The relation between precursor gas and nanotube morphology is not well understood but it was reported that the local heating of a catalyst particle is very important for the extrusion process of a carbon nanotube from a protrusion [12]. The dissociation of different carbonous species is known to be either exothermal or endothermal and would

thus affect the heat distribution on the catalyst surface. Following the described analysis process we extracted the relative abundance of different bundle sizes and plotted them in Figure 26.

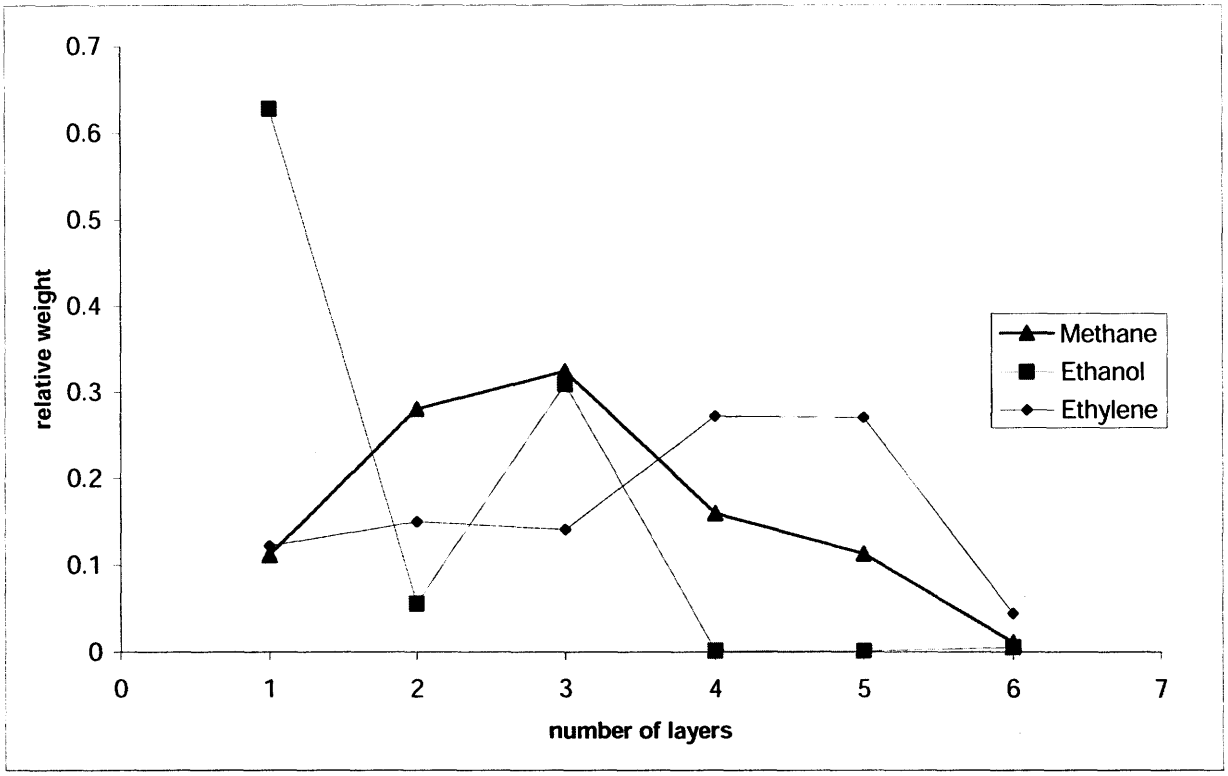

Figure 26 Bundle size for different carbonous precursors

It can be noted that Ethylene produces more bundles whereas nanotubes grown with Ethanol seem to be more individual. This trend is interestingly reflected in the heat of formation (Ethylene 52kJ/mol, Methane -74kJ/mol ethanol -235kJ/mol). Analyzing the first peak we find that the bundles are comprised of different size individual nanotubes with a diameter of (Ethylene 1.2nm, Methane 1.3nm and Ethanol 1.1nm)

4.2. Conditioning of the reactor chamber

It has been previously proposed that carbon nanotube yield during CVD would increase over time. This could be due to catalyst deposition on the reactor walls during synthesis and subsequent improved dissociation of the carbonous precursor by these residues. This conditioning effect was reported from other CVD processes and since iron chloride has a

relatively high vapor pressure (1.1 Torr @194°C) a deposition of the catalyst during the growth phase is perceivable.

Figure 27 shows the yield of nanotubes over the lifetime of a quartz reactor chamber: SEM pictures of grown nanotubes were investigated for the later described analysis of the in-situ rotation experiments. The average number of nanotubes per SEM image could be extracted from this data and the increase in yield over time is negligible as indicated by a slope of 0.5% per experiment.

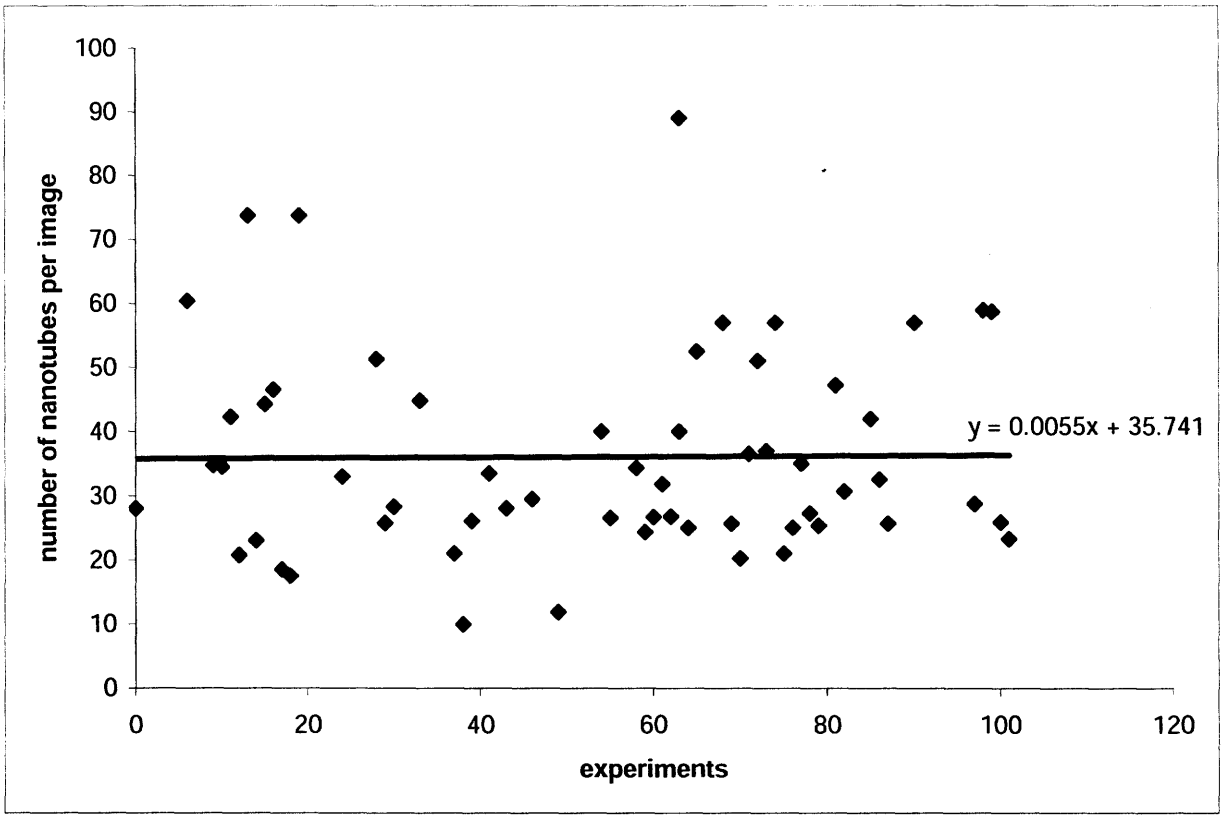

Figure 27 Number of nanotubes vs. number of experiments

Using the described *in-situ* rotation tool, we investigated the fraction of nanotubes that got in contact with the sample during the growth phase. As will be described in a later chapter a significant fraction of the nanotubes only settles after a period of ~5 minutes under the observed conditions (see Figure 35 a). This indicates that the nanotubes which settled during the growth phase must have been floating prior to this time. If we assume a growth speed of 2um/s and an average length of 1mm they must have initiated growth within the first 7 minutes. The fraction of nanotubes that initiated growth during that time

window is plotted in Figure 28

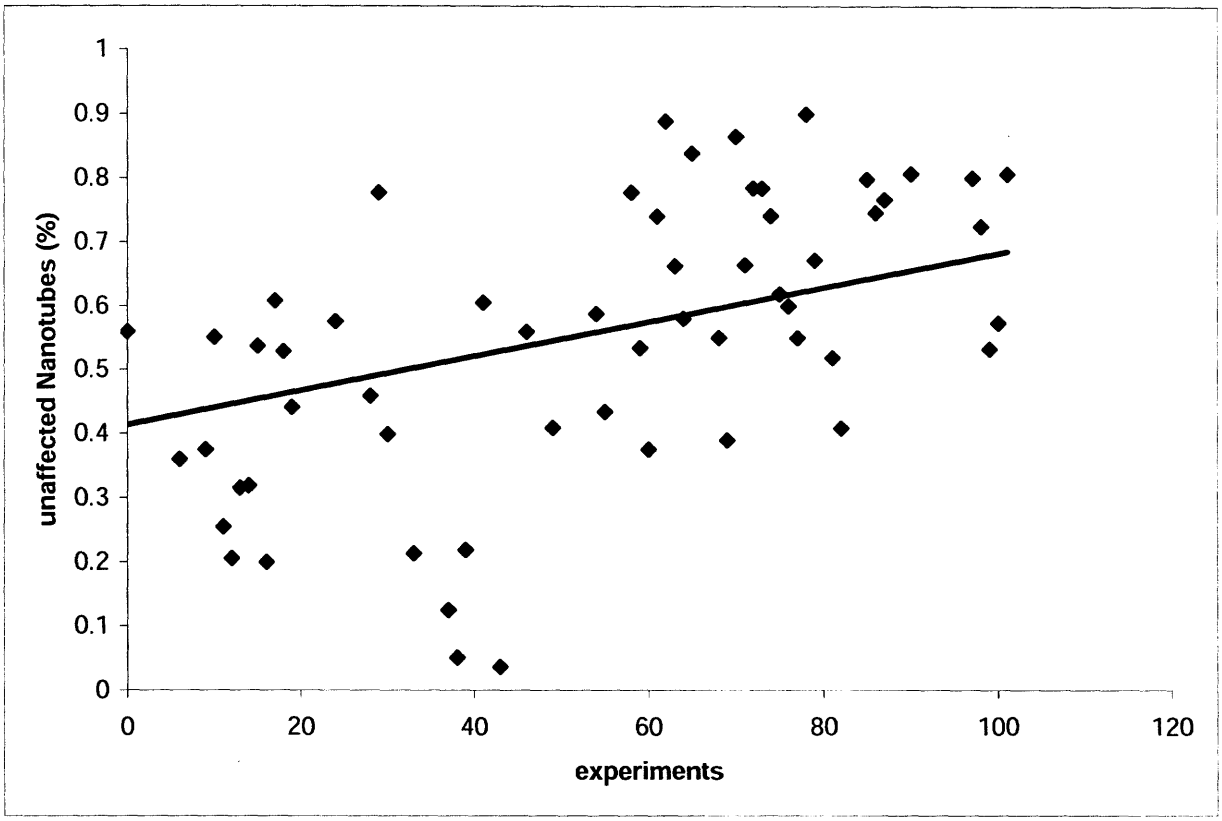

Figure 28 Fraction of nanotubes that settled during the growth phase vs. number of experiments

A clear trend can be seen from the observation of ~10.000 nanotubes: The number of nanotubes that initiated growth early is increasing over the number of experiments. In fact the quartz tube had to be exchanged after ~110 experiments since the fraction of nanotubes that settled during the initial time window was too large to efficiently conduct *in-situ* rotation experiments.

4.3. Optimization of Catalyst

4.3.1. Relation between catalyst size and nanotube size

As previously explained recent reports have shown that the catalyst size and the diameter of nanotubes don't have to correlate. Rather the nanotube would grow from a protrusion

formed on a larger catalyst particle as seen in Figure 29.

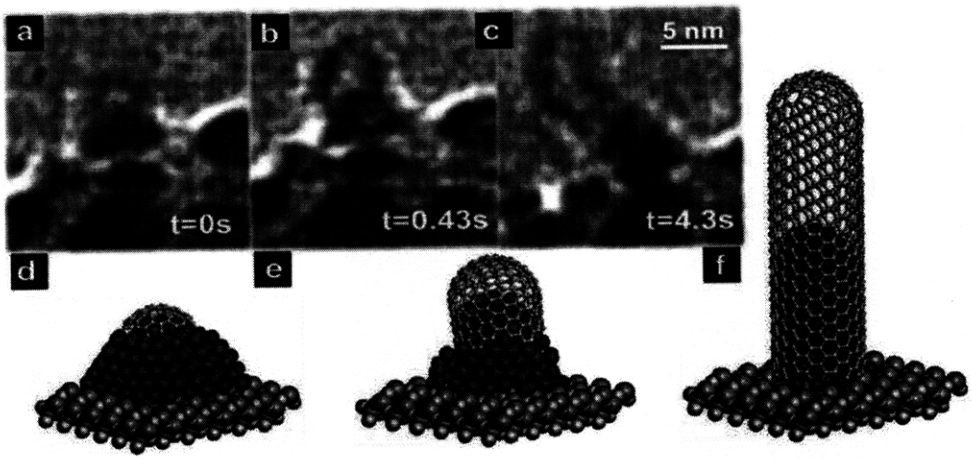

Figure 29 (a-c) In-situ TEM observations and (d-f) simulation of nanotube formation [10]

We provided statistical evidence for this hypothesis in Figure 30 by analyzing the size correlation of 288 nanotubes and the catalyst particles that were attached to one end. It can be seen that the catalyst particles are in general 5 times larger than the nanotube (bundle) they are generating. Furthermore there seems to be no relationship between the nanotube size and the particle.

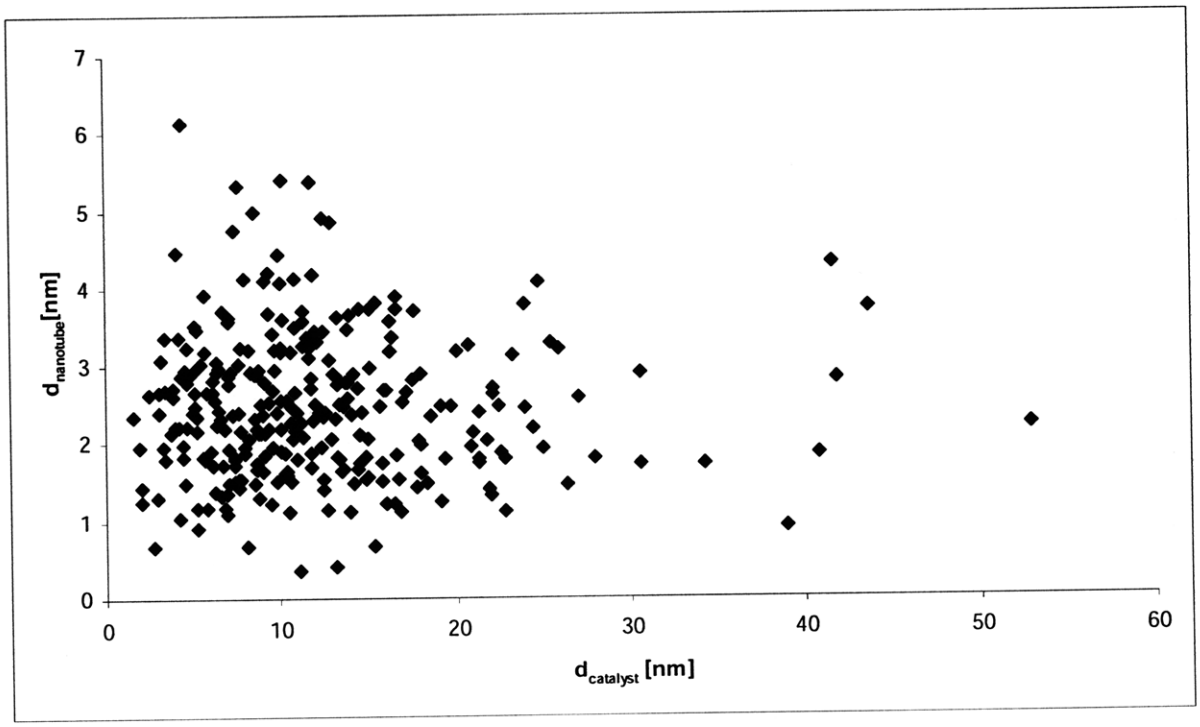

Figure 30 Size of catalyst particles vs. diameter of the nanotube (bundle) grown from it

Taking the height of nanotubes close to the catalyst particle does not seem to avoid the contribution of bundles to the distribution as would be expected if nanotubes would bundle up only after encountering another nanotube.

Indeed it was observed on several occasions that one catalyst particle could extrude several nanotubes (as shown in Figure 31) which raises the question if nanotube bundles are generated by getting their constituents in close vicinity or if they are an inherent catalyst property.

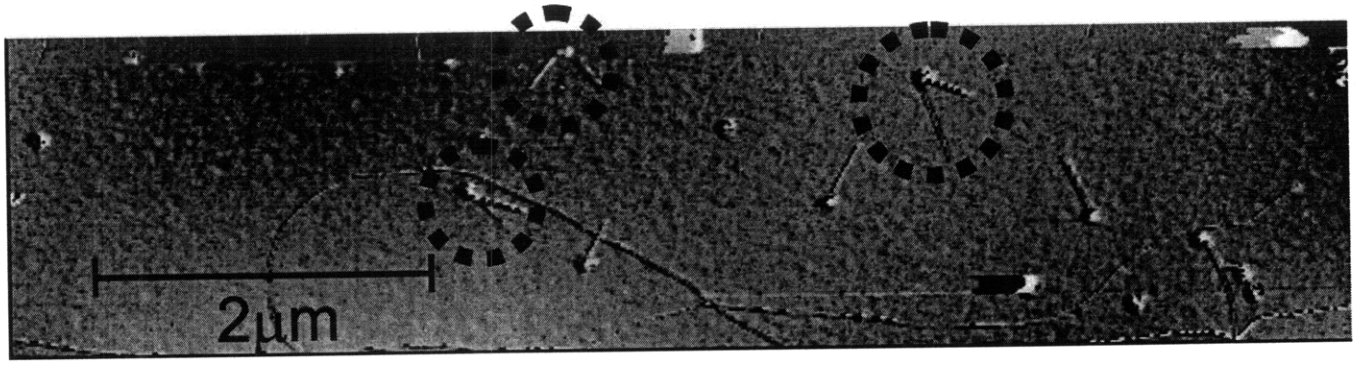

Figure 31 AFM image of multiple nanotube extruding from one catalyst particle

By changing the catalyst density we could generate a region of high nanotube density (14.6 nanotubes per $25um^2$) as well as low nanotube density (2.7 nanotubes per $25um^2$) on the same sample. Since the reaction conditions are the same, the diameter distributions in Figure 32 should give us an indication of the bundling mechanism.

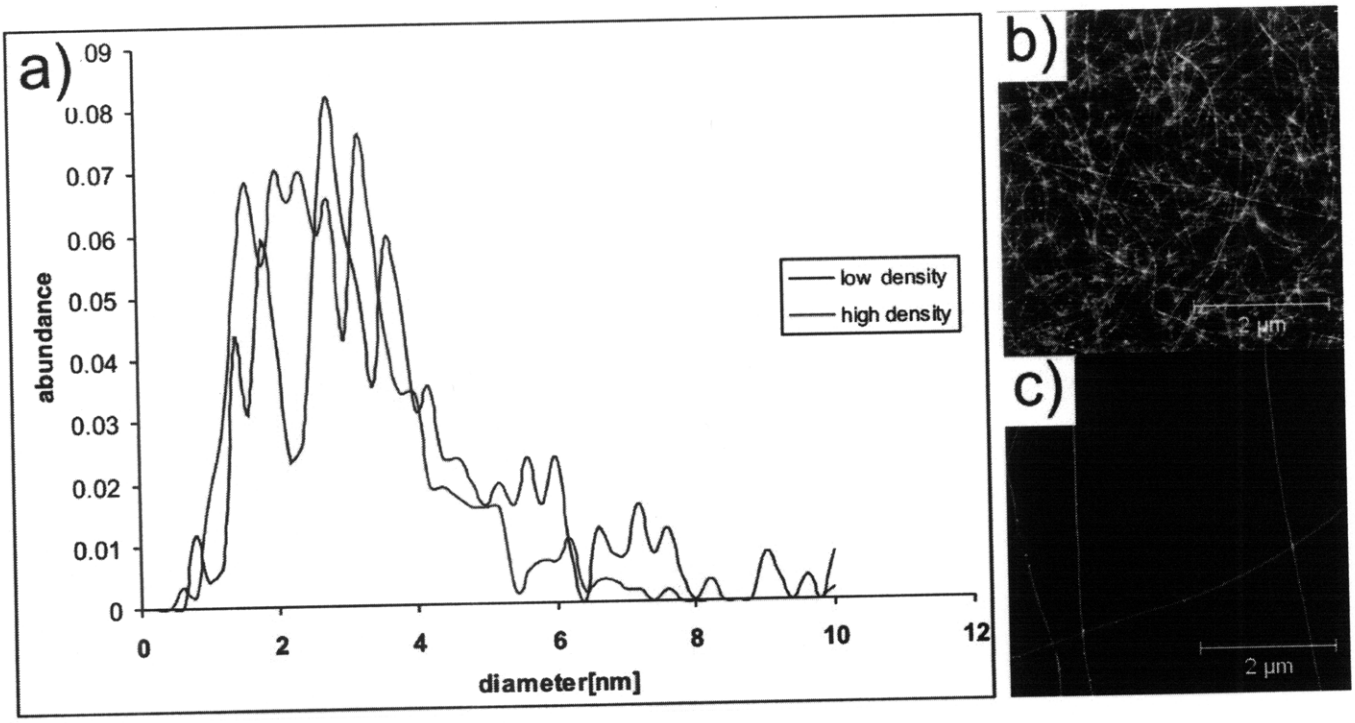

Figure 32 (a) Histogram of two nanotube morphologies on the same sample, representative AFM images of (b) high density and (c) low density

Surprisingly the density of nanotubes does not have a profound effect on the bundle size. This indicates that the previously observed growth of multiple nanotubes from one catalyst particle is responsible for the preferred growth of bundled carbon nanotubes. However, low density nanotubes seem to have a slightly higher probability of forming larger bundles as can be seen by the large diameter tail. This can be understood with another feature that is affected by the density: The high density nanotubes seem to be shorter than the low density ones which gives them less chance to interact with their neighbors to catch another nanotube and form a bundle.

4.3.2. Choice of catalyst

The change of catalyst chemistry is expected to deeply affect the morphology of grown nanotubes: Differences in eutectic temperature, heat release during graphitization, surface tension and so on are major influences on the process of generating nanotubes. Our previous findings indicated that it is possible to influence the number of nanotubes in a bundle within some window but by changing the catalyst we hoped to go beyond these limits. Figure 33 shows the different diameter distributions using our original iron-base

catalyst and a 0.1M solution of copper(II)chloride. The copper-based catalyst growth nanotubes with a much smaller spread and the probability of obtaining larger bundles is much reduced as indicated in Figure 33.

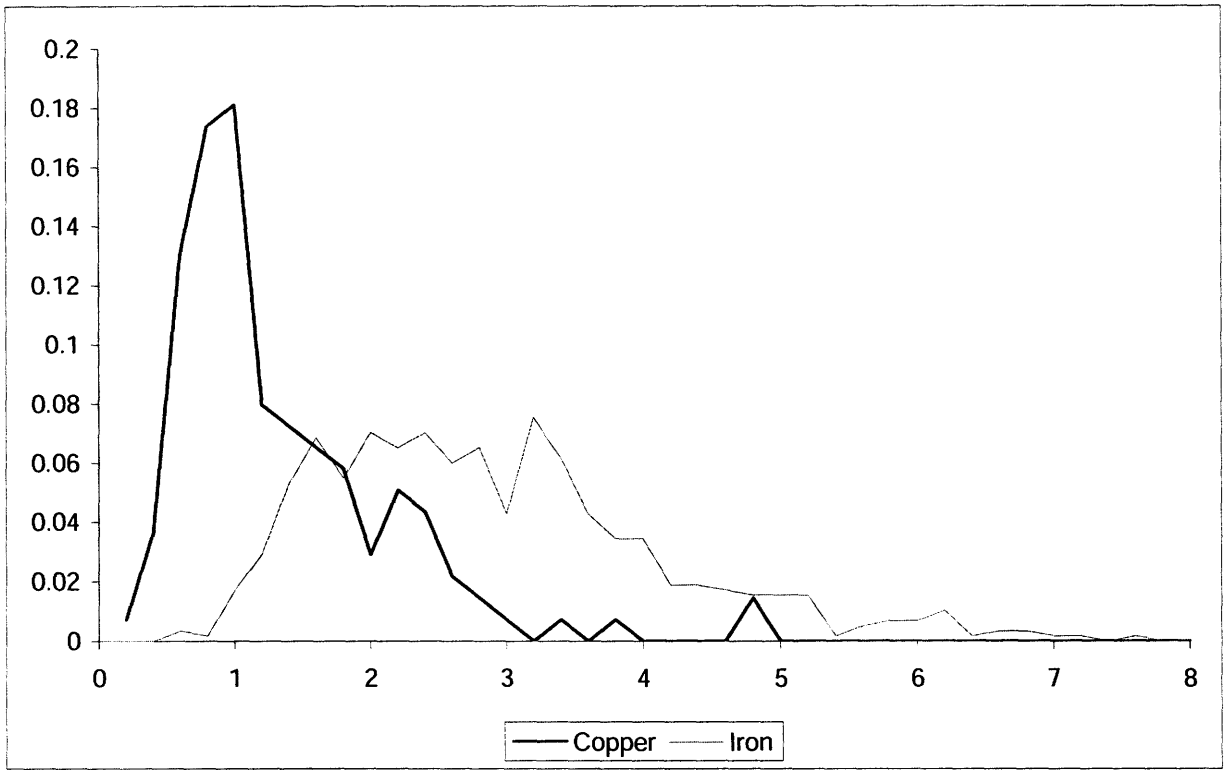

Figure 33 Comparison of diameter distributions obtained with different catalysts

This result should encourage deeper investigation of the tailoring of catalyst particles to obtain a given diameter distribution and bundle size.

5. Fluid dynamics

In the previous chapter we have shown how carbon nanotubes can be synthesized and how optimization in the chemistry is related to their successful growth. However, these findings are not enough to understand the synthesis of ultra long nanotubes. It has been hypothesized that during growth the nanotubes are either partially or totally floating above the substrate, and that this "kite-mechanism" is responsible for achieving ultra long nanotube growth. The exact mechanism that allows nanotubes to float and the reasons they eventually settle to the substrate are still subject to investigation.

Here, we describe a way to use the previously described *in-situ* sample rotation as a tool to statistically investigate the behavior of about 10,000 long aligned nanotubes in a time resolved manner. Once a floating nanotube settles, it experiences a strong enough van der Waals interaction with the substrate so that it will not be affected by the gas flow anymore[13]. By changing the angle between the sample (to which the settled nanotubes are attached) and the gas stream direction that aligns the floating nanotubes, it is possible to distinguish between nanotubes settled before and after the sample rotation.

5.1. Statistical analysis of aligned carbon nanotubes

Figure 34a) shows an SEM image that is representative of our results. There are nanotubes oriented in all three directions, which indicates that nanotubes were still floating and able to align with the gas stream even after their growth was terminated at the end of phase 1. This is a surprising finding considering that previously the growth termination was assumed to coincide with the nanotube getting in contact with the substrate [4].

A typical histogram of the number of nanotubes versus their alignment angle as extracted from the SEM images is shown in Figure 34 b. Normally there can be three peaks observed, corresponding to the nanotubes that settled during the three phases: growth, intermediate and cooling. Integrating the peak area it is easy to calculate the number of nanotubes aligned in a defined direction. The presence of the peak at 0° shows that there is always a certain percentage of the nanotubes settling down during the growth phase.

To evaluate perturbations in the intermediate phase, we define the settled fraction n(t) as the ratio of nanotubes that settled to the substrate during the intermediate phase normalized to the total number of floating nanotubes in the intermediate and cooling phases (i.e., we disregard the nanotubes that already settled during growth phase).

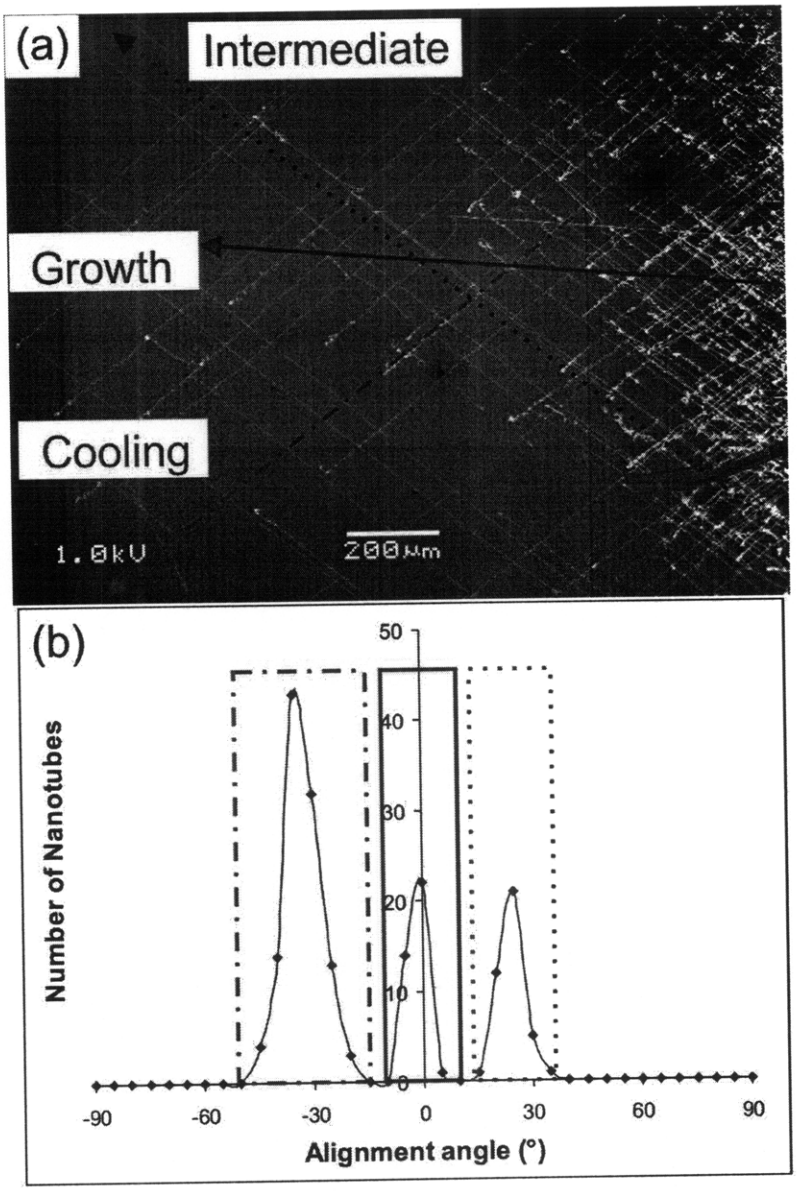

Figure 34 a) SEM picture of the resulting aligned nanotubes with an indication of the gas flow direction for each of the corresponding phases b) Histogram of the angular distribution of the nanotubes with boxes to distinguish each of the phases from left to right: cooling, growth, intermediate phase

In the first set of experiments, the temperature and gas flow were kept constant during the intermediate phase (925°C and 200 sccm Ar) but the waiting time was varied for that

phase. A first important finding is that the settled fraction n(t) increases with time, following an exponential behavior as $n(t)=(1-e^{-\gamma t})$ (Figure 35a). The exponent γ here can be understood as the settling probability for each nanotube, $\gamma = \frac{dn}{dt} \cdot \frac{1}{1-n(t)}$. We term γ the settling rate and observe that it is constant over time..This indicates that the settling of nanotubes is governed by a stochastic process, the probability of a settling event is constant over time and the settling of an individual nanotube is independent of its neighbors, since the decrease in floating nanotubes is linearly dependent on the number of available floating nanotubes (1-n(t)) whereas an influence from the ensemble of neighboring nanotubes would result in a higher order dependence.

The settling does not appear to be triggered by growth termination, disturbance by the rotation process or change of gas mixtures because the settled fraction reaches 0% for the limit of no waiting time after the growth phase .Instead it is only dependent on the duration of the intermediate phase. Therefore processes that occur randomly during growth, such as thermal vibration or flow-induced flutter[14] are likely to be the cause of the settling. I.e. it is perceivable that an oscillatory motion perpendicular to the nanotube axis causes a segment of the nanotube to touch the substrate and subsequently forces the whole nanotube to make contact with the substrate.

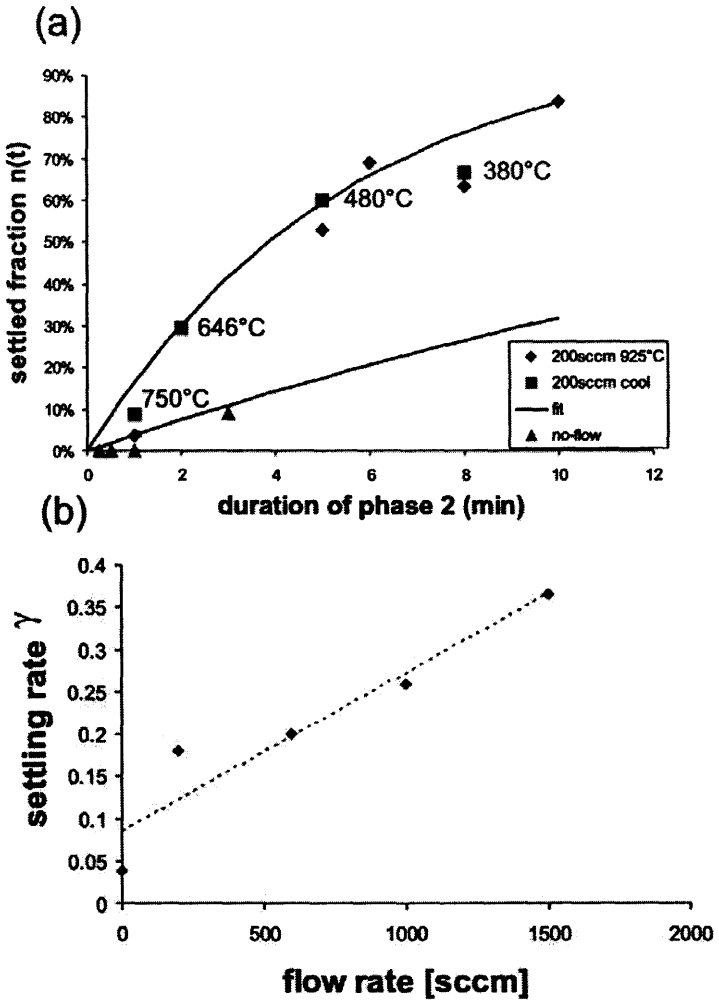

Figure 35 a) Diagram of the settled fraction n(t) over time for growth at 200sccm Argon at 925°C at varying parameters for the intermediate phase (normal, cooling, and static cases for diamond, square, and circle markers respectively). (b) Settling rate γ vs. flow rate and indication that the settling rate is proportional to the flow rate.

5.2. Forces supporting a floating nanotube

Keeping a nanotube floating for longer periods of time in order to allow for long nanotube lengths and higher growth yields requires an understanding of what keeps nanotubes afloat in a gas. To this end we consider the forces acting on a floating nanotube. The three main forces which act on a floating nanotube are gravity, drag from gas flow, and Hooke force arising from the rigidity of the nanotube. The gravitational

force per unit length is constant for a given nanotube. The high rigidity of nanotubes is sufficient to oppose the gravitational force only at short length scales [23] to keep a nanotube from contacting the surface (assuming a cantilevered end on the substrate).

There are two different drag forces acting on a nanotube: A pressure drag caused by a flow perpendicular to the nanotube axis and a surface shear stress from a flow parallel to the axis. Since the nanotube's diameter is small compared to the mean free path of gas molecules, the difference in surface shear stress across a nanotube is going to be negligible and will not be considered.

The pressure drag force, caused by flow perpendicular to the nanotube axis, has two components. First is the obvious flow parallel to the axis of the furnace, which exerts a bending moment on an upward growing tethered nanotube to align it parallel to the gas stream. This is the flow which is considered to be the principal alignment mechanism. Second, and less obvious, is a postulated upward convection flow[24] which arises from a slight difference in temperature between the substrate and the growth gases[25]. The substrate heats the gas adjacent to it, and causes a density gradient which produces an upward flow component that is sufficient to keep the nanotube suspended against the force of gravity and other forces. We refer to this force as a thermal buoyancy force, to distinguish it from the drag force which aligns the nanotubes.

In the following we will investigate the contribution of the different forces on the settling by varying their magnitude.

The settling rate (□) dependence on the flow rate of Ar is plotted in Figure 35 b. It can be seen that the settling rate increases with higher Ar flow rates. Higher flow rates will increase the drag force parallel to the sample surface (while not significantly affecting the vertical drag force), as well as increase the amplitude of the flow-induced flutter[26]. Both effects are expected to increase the settling rate: Larger drag force would deflect the nanotube more and decrease the clearance between the floating nanotube and the substrate. In addition, the larger flutter amplitude could bring a part of the nanotube in contact with the substrate.

The lower limit of our experiment is the static case where the gas flow was turned off during the intermediate phase for varying durations. This eliminates the gas stream induced drag force on the nanotube as well as the flow-induced flutter and only leaves

thermal buoyancy force and rigidity as supporting forces. The observed low settling rate for the static case indicates that the thermal buoyancy generated lift and rigidity are indeed sufficient to support a long, floating nanotube against gravity.

Another important observation from our experiment is that the settling rate does not change if the temperature during the intermediate phase is varied. Even after introducing a continuous cooling by opening the furnace during the intermediate phase, the settling rate is equal to the one obtained at constant temperature as shown in Figure 3a. This means that the significant acting forces have to be independent of temperature. This assumption is surprising especially for the thermal buoyancy induced lift which is expected to have the greatest influence on a floating nanotube. To investigate this hypothesis we conducted temperature measurements with a calibrated K-type thermocouple probe, inserted into the flow through the exit of the tube. The temperature gradient over the sample is indeed a constant over a wide range of furnace temperatures and thus the thermal buoyancy which scales with the temperature gradient would stay constant. After proving the temperature independence of the thermal buoyancy lifting force and assuming the temperature independence of drag force and rigidity, we find that only thermal vibration would have a strong temperature dependence. The amplitude of oscillation caused by thermal vibration would increase for higher temperatures and would thus affect the settling rate. We conclude that thermal vibration can be excluded as the determining stochastic process for settling.

To prove that an interaction between the nanotube and the fluid is the key parameter to keep nanotubes afloat a mild vacuum (~200mbar) was generated for 30 seconds. This perturbation decreases the drag force, which is proportional to gas density, and only leaves nanotube rigidity to support itself. Since the observed nanotubes have extremely high aspect ratios this force should not be sufficient and indeed the settled fraction was increased to nearly 100% after pumping out the gas (compare Figure 36 a). The corresponding angle distribution does not exhibit a peak in θ_3 direction since all the floating nanotubes were settled by pumping Figure 36b. This is an important finding since it enables us to reliably settle all floating nanotubes and terminate their growth process at a given time by pumping. This makes time-resolved studies of other aspects of nanotube growth possible in the future.

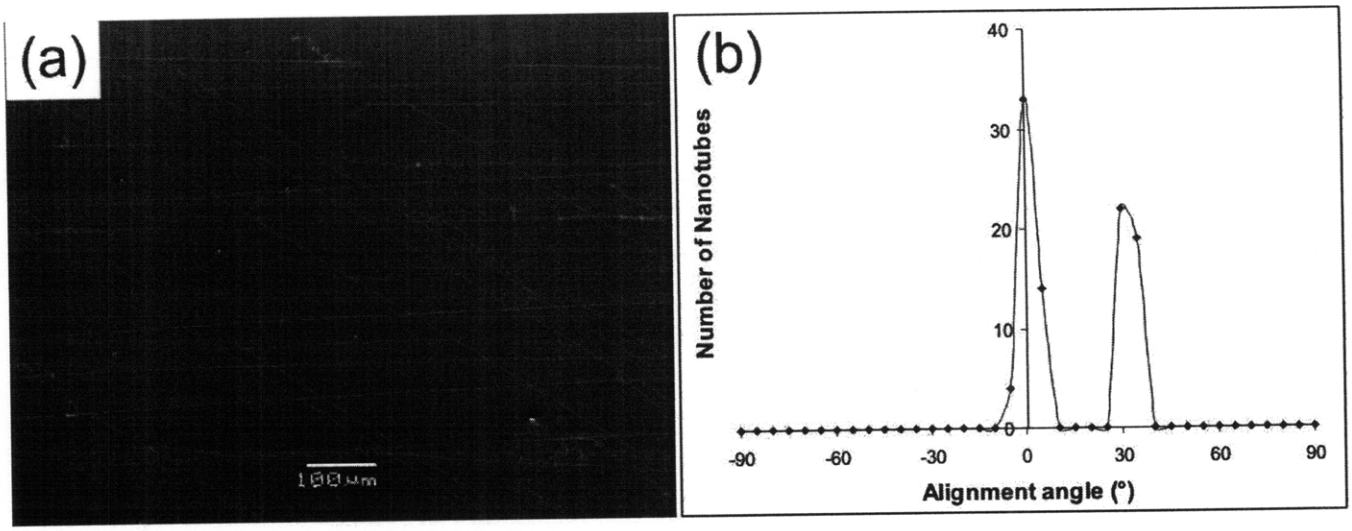

Figure 36 (a) SEM picture of the nanotube orientation obtained after pumping and (b) corresponding histogram

5.3. Observations on individual nanotubes

Apart from information on nanotube behavior based on statistical examination, our time-resolved analysis also generated instructive results from observation of individual nanotubes. The growth mechanism, amongst others, can be elucidated by our experiments. Depending on which section of the nanotube is being lifted up, either "partial-" or "total-" floating mechanisms were proposed previously. The first mechanism proposes the downstream end of the nanotubes being lifted up ("partial floating") with the other part of the nanotube in contact with the substrate[27] [4]. The other mechanisms (either tip- or base-growth) suggest that the whole nanotube is floating while its upstream end is tethered to the substrate. In our observations, most of the nanotubes have their entire length aligned along only one direction. This supports the "total-floating" mechanism, since the partial floating mechanism would allow for kinks as segments are aligned in different directions. This observation agrees with findings of Huang et al.[13].

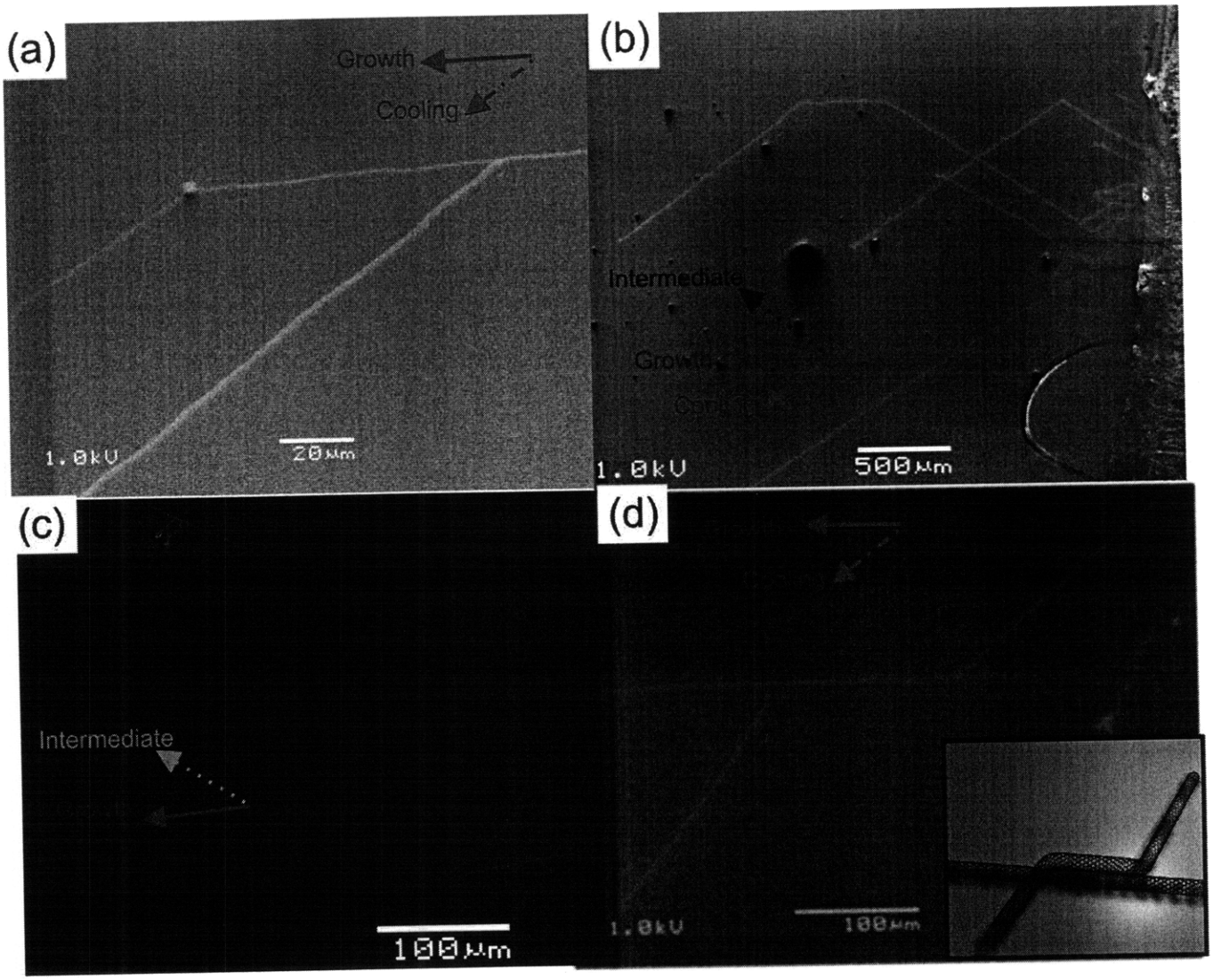

Figure 37 (a,b) Nanotubes exhibiting kinks, (c) curvature (d) bundling with inset illustrating the shape of the bundled nanotubes. Origins of each arrangement are discussed in the text

However, on a number of occasions we do observe nanotubes having sections aligned along different directions that are joined by sharp kinks (Figure 37a-b), which indicates that a part of the nanotube had already settled during a previous phase while other segments became aligned along a new direction with subsequent gas flow. In these cases, usually the upstream end of the nanotube settled during an earlier phase than the downstream end, in agreement with observations by Geblinger et al.[28]. This behavior challenges the picture of a vibrating nanotube that is floating parallel to the substrate, since the oscillation amplitude perpendicular to the nanotube axis should be largest at the downstream end and contact to the substrate should happen more often at the downstream

end.

In order to elucidate this, we carried out experiments to determine the distance between the floating nanotube and substrate. For this a SiO_2 chip was positioned perpendicular to the growth substrate as indicated in Figure 5a. During the intermediate phase the chip was moved across the growth substrate with the previously used manipulator setup.. The nanotubes grown on the first sample are expected to get in contact with the moving substrate and adhere there due to van-der-Waals forces. The shape of the nanotubes on this substrate would reflect a perpendicular projection of the floating nanotubes (Figure 38 a). The flow perturbations from this process are believed to not affect the overall shape of the floating nanotube since the imaging substrate is much larger than the nanotube and it thus generates a homogeneous distortion along the whole nanotube. However, it can be noted from Figure 38 b) that most captured nanotubes exhibit curls along their length which we explain by insufficient alignment between nanotube and imaging substrate: If the nanotube was pointing towards the imaging substrate its projection on the substrate would be shortened and the excess length of the nanotube could roll up as observed. Only focusing on the unperturbed nanotubes we found evidence that the clearance between the nanotube and the growth substrate is between 100 and 500μm. With these findings the vibration amplitude of the downstream end would have to be substantial to force it to bind onto the substrate. A higher order mode of the oscillation, however, could cause a larger amplitude close to the anchoring point of the nanotube which makes the upstream part touch the substrate.

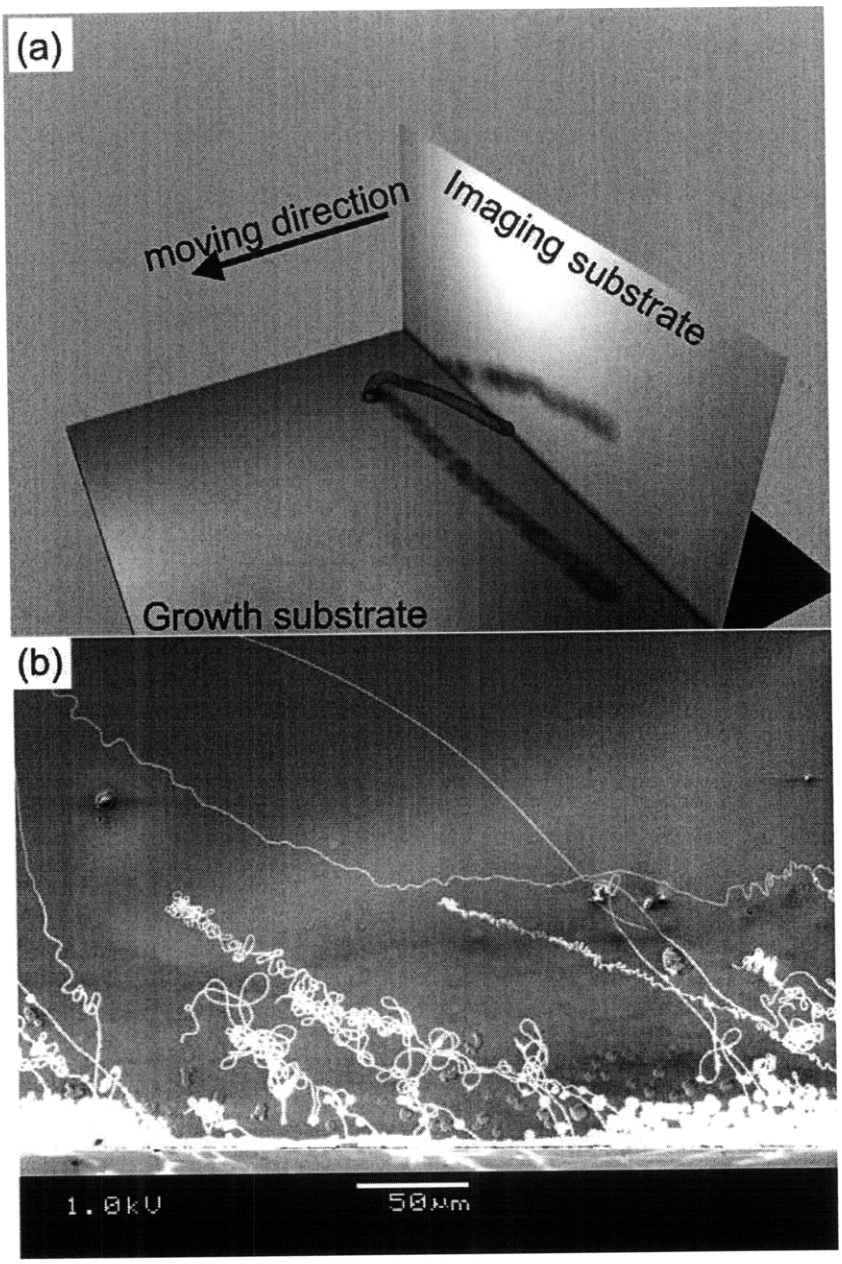

Figure 38 (a) Sketch of the experimental procedure (b) SEM picture of carbon nanotubes in contact with a substrate perpendicular to the growth substrate

Some nanotubes exhibit a curvature rather than a kink as they transition from one direction to the other if the angular velocity of the rotation is lowered (Figure 37b). This is indicating that the tube is in the process of settling while the sample was rotated. From the rotation speed we can estimate that the velocity of the contact point "zipping" towards the downstream end is on the order of ~25µm/s.

Occasionally nanotubes form bundles as shown in Figure 38d. The segments of the latter

grown nanotube are here seen to be bundling with another already settled nanotube. We attribute this observation to the following mechanism: The motion of the interface between the floating nanotube and its settled segments can be guided by an obstacle such as another nanotube. Subsequently a bundle is formed between the two nanotubes with an orientation equivalent to the already settled nanotube. The force on the floating segment acting in the direction of the gas stream can overcome the nanotube-nanotube interaction at a later time and can once again separate the two tubes. This mechanism is also understood to be responsible for nanotube alignment along crystallographic directions or step edges[28].

The sample rotation tool not only allows us to characterize the nanotube growth and settling mechanism, but also helps evaluate the potential for integration of flow aligned nanotubes into electronic applications. The efficiency of alignment is demonstrated by a narrow angular deviation in Fig 2b (usually around 15 degrees from our experiments) which shows that, if further improved, gas flow alignment could rival the efficiency of electric field-assisted alignment (7°) for long nanotubes[29].

Lastly, it should also be noted that the settled fraction reaches 100% (meaning all nanotubes settled) typically after a waiting period of more than 10 min (see Figure 35 a). Since our CVD synthesis time is 20 minutes, the majority of the floating nanotubes must have initiated growth within the second half of the CVD process (phase (1)). This renders most calculations for the growth speed of nanotubes incorrect, since it is assumed that the growth duration coincides with the time of the start of the CVD process. This is also consistent with our finding that increasing the synthesis time above 10 minutes only affects the density of long aligned nanotubes but not the average length. At present it is still not clear why some nanotubes initiate growth only after 1h of synthesis time and more detailed investigation of the catalyst particle has to be carried out.

In conclusion, using the relatively simple and easily available process of in-situ sample rotation, we contribute several new findings to the picture of growing nanotubes. Long nanotubes can be reliably aligned with the gas flow and are completely floating over the substrate with the upstream end tethered on the surface. Using tube alignment as a characterization parameter we investigated the process of nanotube settling and found that it is determined by a stochastic process. The rate of settling is affected by process

parameters that are related to the different forces acting on a nanotube. The settling process can be described by a "zipper"-like motion of the interface between the settled and floating segment of a nanotube directed towards the downstream end with a speed of ~25um/s. The clearance between floating nanotubes and the substrate is on the order of several hundred micrometers. These new understandings, as well as the in-situ rotation tool will open up further opportunities in optimizing the CVD synthesis process and the future integration of nanotubes in circuits.

6. Conclusions

In this work we show evidence for the occurrence of carbon nanotube bundles based on several analysis techniques: Raman spectroscopy probes individual nanotubes but can sometimes provide proof for several resonant nanotubes within a bundle. Electrical transport measurements show that combined nanotubes can provide high current carrying capabilities.

AFM observation cannot only give anecdotal evidence of occurring bundles but by using statistical data in form of diameter distributions we can extract much more information about nanotubes within a bundle than with other techniques.

The optimization of growth parameters, aimed towards generating individual nanotubes as well as ultra long nanotubes, was partially successful and nanotubes with lengths of several millimeters could be reliably produced.

These ultra long nanotubes were used to investigate the fluid dynamical interaction of nanotubes and the gas stream and information about the settling were obtained using a novel in-situ rotation tool.

References

1. Esquivel, E.V. and L.E. Murr, *A TENT analysis of nanoparticulates in a Polar ice core.* Materials Characterization, 2004. **52**(1): p. 15-25.
2. Murr, L.E., et al., *Carbon nanotubes, nanocrystal forms, and complex nanoparticle aggregates in common fuel-gas combustion sources and the ambient air.* Journal of Nanoparticle Research, 2004. **6**(2-3): p. 241-251.
3. Iijima, S., *Helical Microtubules of Graphitic Carbon.* Nature, 1991. **354**(6348): p. 56-58.
4. Zheng, L.X., et al., *Ultralong single-wall carbon nanotubes.* Nature Materials, 2004. **3**(10): p. 673-676.
5. Endo, M., M.S. Strano, and P.M. Ajayan, *Potential applications of carbon nanotubes*, in *Carbon Nanotubes.* 2008. p. 13-61.
6. Geim, A.K. and K.S. Novoselov, *The rise of graphene.* Nature Materials, 2007. **6**(3): p. 183-191.
7. Harutyunyan, A.R., et al., *Hidden features of the catalyst nanoparticles favorable for single-walled carbon nanotube growth.* Applied Physics Letters, 2007. **90**(16).
8. Kukovitsky, E.F., et al., *Correlation between metal catalyst particle size and carbon nanotube growth.* Chemical Physics Letters, 2002. **355**(5-6): p. 497-503.
9. Nasibulin, A.G., et al., *Correlation between catalyst particle and single-walled carbon nanotube diameters.* Carbon, 2005. **43**(11): p. 2251-2257.
10. Hofmann, S., et al., *In situ observations of catalyst dynamics during surface-bound carbon nanotube nucleation.* Nano Letters, 2007. **7**(3): p. 602-608.
11. Lin, M., et al., *Direct observation of single-walled carbon nanotube growth at the atomistic scale.* Nano Letters, 2006. **6**(3): p. 449-452.
12. Moshkalev, S.A. and C. Verissimo, *Nucleation and growth of carbon nanotubes in catalytic chemical vapor deposition.* Journal of Applied Physics, 2007. **102**(4): p. 6.
13. Huang, L.M., Z. Jia, and S. O'Brien, *Orientated assembly of single-walled carbon nanotubes and applications.* Journal of Materials Chemistry, 2007. **17**(37): p. 3863-3874.
14. Hertel, T., R.E. Walkup, and P. Avouris, *Deformation of carbon nanotubes by surface van der Waals forces.* Physical Review B, 1998. **58**(20): p. 13870-13873.
15. Araujo, P.T., et al., *Third and fourth optical transitions in semiconducting carbon nanotubes.* Physical Review Letters, 2007. **98**(6): p. -.
16. Javey, A., et al., *Ballistic carbon nanotube field-effect transistors.* Nature, 2003. **424**(6949): p. 654-657.
17. Yao, Z., C.L. Kane, and C. Dekker, *High-field electrical transport in single-wall carbon nanotubes.* Physical Review Letters, 2000. **84**(13): p. 2941-2944.
18. Wang, X.F., et al., *Field-effect transistors based on single-wall carbon nanotubes bundles.* Chinese Journal of Electronics, 2005. **14**(4): p. 599-602.
19. Ye, Y., et al., *Hydrogen adsorption and cohesive energy of single-walled carbon nanotubes.* Applied Physics Letters, 1999. **74**(16): p. 2307-2309.
20. Tersoff, J. and R.S. Ruoff, *STRUCTURAL-PROPERTIES OF A CARBON-NANOTUBE CRYSTAL.* Physical Review Letters, 1994. **73**(5): p. 676-679.
21. Reina, A., et al., *Growth mechanism of long and horizontally aligned carbon*

nanotubes by chemical vapor deposition. Journal of Physical Chemistry C, 2007. **111**(20): p. 7292-7297.

22. Hofmann, S., et al., *Surface diffusion: The low activation energy path for nanotube growth.* Physical Review Letters, 2005. **95**(3): p. 5.
23. Wong, E.W., P.E. Sheehan, and C.M. Lieber, *Nanobeam mechanics: Elasticity, strength, and toughness of nanorods and nanotubes.* Science, 1997. **277**(5334): p. 1971-1975.
24. Jin, Z., et al., *Ultralow feeding gas flow guiding growth of large-scale horizontally aligned single-walled carbon nanotube arrays.* Nano Letters, 2007. **7**(7): p. 2073-2079.
25. Cheng, T.S. and M.C. Hsiao, *Computation of three-dimensional flow and thermal fields in a model horizontal chemical vapor deposition reactor.* Journal of Crystal Growth, 2006. **293**(2): p. 475-484.
26. Schouveiler, L., C. Eloy, and P. Le Gal, *Flow-induced vibrations of high mass ratio flexible filaments freely hanging in a flow.* Physics of Fluids, 2005. **17**(4): p. -.
27. Huang, S.M., et al., *Growth mechanism of oriented long single walled carbon nanotubes using "fast-heating" chemical vapor deposition process.* Nano Letters, 2004. **4**(6): p. 1025-1028.
28. Geblinger, N., A. Ismach, and E. Joselevich, *Self-organized nanotube serpentines.* Nat Nano, 2008. **3**(4): p. 195-200.
29. Hongo, H., F. Nihey, and Y. Ochiai, *Horizontally directional single-wall carbon nanotubes grown by chemical vapor deposition with a local electric field.* Journal of Applied Physics, 2007. **101**(2).